Switching-Based State-of-Charge Estimation of Lithium-Ion Batteries

by

Yingchen Su

A Thesis Submitted in Partial Fulfillment of the Requirements for the Degree of
Master of Science in Mechanical Engineering

Advised by

Dr. Tuhin Das, Assistant Professor, Mechanical Engineering
Department of Mechanical Engineering
Kate Gleason College of Engineering
Rochester Institute of Technology
Rochester, New York
July 2011

Approved By:

Dr. Tuhin Das,
Assistant Professor, Mechanical Engineering
Advisor _____

Dr. James E. Moon,
Associate Professor, Electrical Engineering _____

Dr. Brian J. Landi,
Assistant Professor, Chemical Engineering _____

Dr. Wayne Walter,
Professor, Mechanical Engineering
Department Representative _____

Thesis Release Permission Form

Rochester Institute of Technology

Kate Gleason College of Engineering

Switching-Based State-of-Charge Estimation of Lithium-Ion Batteries

I, Yingchen Su, hereby grant permission to the Wallace Memorial Library reproduce my thesis in whole or part.

Yingchen Su

Date

Acknowledgments

I would like to acknowledge the invaluable encouragement from my parents, family, and friends. I am wholeheartedly thankful for my advisor, Dr. Tuhin Das. His guidance, encouragement, and support helped me to grow. I would also like to thank Dr. Brian J. Landi and his student Matthew Ganter for conducting part of the experiment for us. Finally, I would like to thank my labmates, W. John Nowak and Steve Snyder, for making the lab a better place for work. This work was supported by the Office of Naval Research under grant #N000140910272.

Abstract

The objective of this thesis is to explore a switching-based approach to estimate the state of charge (SOC) of Li-ion batteries. The knowledge of SOC can be utilized to significantly enhance battery performance and longevity. The thesis first presents a brief discussion on various SOC estimation methods, such as coulomb counting, use of electrochemical model combined with Kalman Filtering and open-circuit voltage (OCV). Subsequently, emphasis is placed on the OCV-based method. The advantage of the OCV method lies in its simplicity. It obviates the need for modeling and lowers computational burden compared to model-based approaches. The method yields accurate SOC estimates if a long period of battery resting time (switch-off time) is allowed. For smaller switch-off durations, the accuracy of SOC estimation reduces. However, experiments show that Li-ion batteries could give acceptable SOC estimates due to their fast transient response during switch-off. In traditional usage scenarios, a switch-off interval may not be practical. However, in distributed power systems with multiple storage elements, a switch-off interval could be provided. Experiments are conducted to characterize the estimation error versus the switch-off time. To reduce the switch-off time to 30 second switch-off time and to increase the accuracy of SOC estimation, a method is proposed to extrapolate the OCV at infinite time from the measured OCV using a time constant. This leads to a predicted OCV for infinite switch-off intervals. Experiments are conducted to confirm the improved SOC estimation using the proposed method. For experimentation, a commercially available $LiFeMgPO_4$ battery module as well as a single cell $LiFePO_4$ battery, is used.

Contents

List of Figures

Nomenclature

SOC	State of charge
$LiFeMgPO_4$	Lithium iron magnesium phosphate
$LiFePO_4$	Lithium iron phosphate
SOH	State of health
OCV	Open circuit voltage
V_{oc}	Open-circuit voltage
EMF	Electromotive force
EKF	Extended Kalman filter
V_{dl}	Battery diffusion voltage (V)
C_{dl}	Battery internal capacitance (F)
CA	Cathode
AN	Anode
$RMSD$	Root mean square deviation
τ	Battery time constant (sec)
$SOFC$	Solid oxide fuel cell
P_{dem}	Power demand (W)
P_{fc}	Fuel cell power (W)
P_{uc}	Ultra-capacitor power (W)
P_{ba}	Battery power (W)
DC	Direct current
AC	Alternative current
R	Resistance

Chapter 1

Introduction

1.1 Motivation

As the rate of technological advancement has increased in recent decades, the demand for energy has grown rapidly. However, many energy resources such as coal and petroleum are harmful to the environment and have limited supply. Alternative energy resources that are more environmentally friendly than petroleum and coals, such as fuel cells, wind turbines, solar cells, etc. have been an active field of research. For optimal performance, alternate energy resources are typically hybridized with energy storage devices. Hence, the ability to effectively manage generation and storage of energy becomes a necessary task to accomplish. One of the most common energy storage devices is the rechargeable battery. In order to extend the lifetime of a battery, enhance performance, and improve reliability, an accurate state of charge (SOC) determination method is required. An example of SOC estimation application is in electric vehicle. Having the knowledge of the battery's SOC can efficiently run the electric motor by charging the battery above certain valid limits.

Over the years of battery technology development, various SOC determination methods have been developed. A summary of techniques for SOC determination is listed in [10]. Authors of [11] also present an extensive review of battery SOC estimation techniques. They list methods such as open- circuit voltage (OCV) measurement, electromotive force (EMF) method, book-keeping systems and adaptive systems. [11] presents the advantages and drawbacks of different methods that can be applied to different types of batteries such

as lead acid, nickel metal hydride and lithium ion batteries.

Currently, the most promising type of battery for future energy storage applications is the Li-ion battery [12]. It has many applications; however, the biggest drawback of Li-ion batteries is the safety issue. Lithium ion batteries are not as reliable as nickel metal hydride, nickel-cadmium or lead acid due to their poor heat dissipation property [13]. Without the ability to monitor SOC, overcharging or overdischarging the battery can occur. If the battery is overcharged, thermal runaway and a potential fire hazard can occur. In some extreme cases, if the battery is overheated and overcharged, the battery can explode. If the battery is overdischarged, an irreversible new chemical reaction can occur in the battery, resulting in new compounds in the battery. This either leads to reduction of battery capacity or makes the battery system non-operational [14]. Therefore, for safety and battery protection, the ability to monitor the state of charge of batteries, especially lithium-ion batteries, becomes critical. To make use of the lithium-ion battery system in an energy system, combined SOC estimation and energy system management present a challenging task.

1.2 Literature Review

In the field of battery management, SOC estimation is an ongoing field of research. There are several techniques used for SOC determination in various applications. Examples of SOC estimation techniques include: coulomb counting method, utilizing battery electrical properties (capacitance, impedance, electromotive force (EMF)) and open-circuit voltage (OCV) [11].

The traditional simple coulomb counting method is an open-loop SOC estimator. It utilizes the knowledge of the charging or discharging current and by integrating the current over time, estimates the coulomb count. The SOC is estimated by subtracting the total charge flow from the initial 100% available charge. It can be accurate and cost effective if the proper battery model is applied [15].

The coulomb counting method often depends on the current flowing from the battery to

external circuits; therefore, the accuracy of this method depends on the pre-existing knowledge of the external circuitry and battery parameters such as the amount of charge in a fully charged cell. Substantial error can accumulate if the system does not account for self-discharge current or the Columbic efficiency of the battery. In addition, the simple coulomb counting method does not consider the aging effect of the battery [15]. Modifications have been proposed to improve the accuracy of the coulomb counting method. In [16], Ng et.al propose a coulomb counting method for estimating SOC by utilizing the charging and discharging rate of the battery. In [17], an optimized support vector machine SOC estimator is created by utilizing a traditional coulomb counting estimation method and real-time pattern recognition technique. The authors have demonstrated an accurate result but it requires a period of training time for the SOC estimator to be accurate. In [18], the authors report the development of mathematical models that describe the EMF, overpotential functions and SOC by utilizing a simple coulomb counting method. They use the open-circuit voltage measurement and current measurement with their battery model to create a battery SOC indication system. They have discovered that it is more accurate to use the open-circuit voltage method, but the method does not provide continuous indication of the SOC since the battery needs to rest for some period of time.

Another SOC estimation method is one that uses the equivalent circuit model of the battery. The model uses electrical properties such as impedance, capacitance and EMF of the battery. By fitting parameters to test data, circuit parameter values can be determined [19, 20]. An equivalent circuit model captures the transient characteristics of a battery. Furthermore, by gaining an understanding of the parameter variations, one can also estimate the state of health of the battery [21]. The equivalent-circuit-based SOC estimation method is commonly implemented in battery management systems [5, 16, 22, 23]. An example of utilizing the equivalent circuit model for SOC estimation is shown in [23]. Here, the authors adopted a battery equivalent circuit model in conjunction with a pattern recognition algorithm to estimate SOC.

Similarly, battery electrical properties are also used to develop analytical models that

relate current, voltage and SOC. In [24], such an analytical modeling approach is developed for SOC determination. The authors additionally take the temperature and the cycle aging effects into consideration in their model. Battery electrical properties have also been used to develop analytical models relating EMF, battery internal resistance and SOC [22, 25, 26]. In [25], a dynamic analytical battery model is developed using the knowledge of EMF and internal resistance. The authors use a microprocessor to store lookup tables of voltages, currents, and temperature factors for an accurate online SOC estimation based on measurements. The work in [22] focuses on combining EMF and coulomb counting methods for a faster and more accurate result. Similar to the work done in [25], the authors in [22] incorporate impedance, load current and terminal voltage to estimate SOC. Another example utilizing battery parameters for SOC estimation is in using the impedance of the battery to estimate the SOC, as done in [26]. It is noted that since the impedance parameter varies from battery to battery, this method can only be used for a given battery with known parameter values obtained through test data. In [27], the dynamic behavior of batteries such as impedance variation and frequency response during operation are analyzed to determine SOC.

The common drawback of using electrical properties to estimate SOC is that a specific type of battery chemistry is assumed. The electrical characteristic such as battery impedance and capacitance changes as the operating conditions change. The battery characteristic does not stay the same over time even with the same type of chemistry. The variation is greater if the battery chemistry or operational temperature changes.

Another approach to SOC estimation is using the electrochemical model of the battery. In this regard, the Li-ion chemistry has been considered in a number of papers [4, 28–32]. The electrochemical model is more accurate than the equivalent circuit model since the electrochemical model takes into account different lithium ion battery chemistries and temperature effects. The advantage of this method is the accuracy of the SOC estimation in real time. However, the method could be computationally intensive. A number of

researchers have reported techniques to increase the speed of the simulation for the electrochemical model in order to apply the model in practice. Two reduced-order lithium ion battery models are introduced in [33]. They demonstrate an accurate model for SOC estimation without a lengthy computational time. This model allows real-time implementation in practice with some sacrifice in accuracy.

Many research groups have investigated the approach of using the open-circuit voltage (OCV) of a battery to estimate SOC. The OCV method is widely implemented in SOC estimation algorithms. The basic principle of the OCV method relies on the thermodynamic equilibrium of lithium ion cells. As the lithium ion cell reaches its thermodynamic equilibrium, the lithium chemical potential (ionic and electronic) difference between the anode and the cathode is commonly known as the open-circuit voltage (OCV). The OCV is a function of chemical composition, pressure and temperature as presented in [34]. It is an electrical representation of the batteries' chemical reaction.

Authors of [35] have conducted extensive testing to obtain OCV versus SOC behaviors of lead-acid batteries. They assume a constant operational temperature of $25°$C. All batteries are fully charged before the discharging tests. The error is less than 3% after a two-minute open-circuit interval for the discharge test. For the charging state, the error is less than 5% after a ten-minute open-circuit interval. The authors show that it takes a period of time to estimate SOC accurately using OCV measurement. In [36], the authors utilize a modified OCV-SOC relationship based on conventional OCV-SOC to estimate SOC of lithium-ion batteries. The authors acknowledge that the traditional open-circuit voltage method is accurate, but needs a rest time to estimate the SOC. They use an extended Kalman filter with optimum adaptive algorithm to minimize the SOC estimation error based on the OCV vs. SOC curve. An equation relating OCV with the terminal voltage of the battery is presented in [11]. The authors reviewed the work of many groups that have utilized SOC-OCV relationship, such as [37]. Research groups often used the OCV estimation method instead of direct measurement to avoid switching off the battery from

the system. Equation (1.1) is commonly used for SOC estimation, where V_{term} is the battery terminal voltage, and is directly measurable. The approach uses the terminal voltage to determine the OCV and subsequently uses a map between OCV and SOC to estimate the SOC. In [38], the authors utilize Equation (1.1) for OCV estimation without switching off the battery. The accuracy of using the OCV estimation can vary depending on the current SOC of a battery. In addition, Equation (1.1) does not take into consideration the hysteresis that occurs in lithium ion batteries [1, 9]. Research groups have investigated various modifications of the OCV estimation technique.

$$OCV = V_{term} + IR \tag{1.1}$$

Examples of OCV estimation technique can be found in the following papers: in [39], an algorithm is developed for SOC estimation that incorporates EMF and current to estimate OCV. Furthermore, in [40], the authors demonstrate that the OCV can provide a basis for SOC measurement and utilized the OCV vs. SOC property to perform cell equalization of the battery. In [41] and [42], an equivalent circuit model is used for OCV estimation. Using the SOC vs. OCV relationship curve, the SOC of the battery is estimated. A sliding mode observer is designed in [42] for estimating the electrical properties and OCV of the battery. In [43] also, an equivalent circuit model is utilized for OCV estimation. In this paper, the authors propose to use a time constant to estimate OCV and apply it to a dynamic model of the EKF algorithm using a Kalman filter. In [44] and [45], the authors model the battery to account for temperature and thermal effects. They estimate the open-circuit voltage to find SOC. Their model is less accurate at low temperatures and at high discharge rates. With the knowledge of temperature effects, authors in [46] investigated temperature effects on battery parameters such as OCV, resistance and capacitance. By incorporating an Extended Kalman filter (EKF) algorithm into their battery data, they have designed an accurate SOC estimation under temperature variation.

The open-circuit voltage SOC estimation technique has been well established by various research groups because of many advantages of this method. One advantage, such as

the result shown in [47], shows that the OCV versus SOC curve is independent of the age of the Li-ion battery. The OCV method can be very accurate if a rest time of the battery is allowed [36][48]. The relationship of OCV versus SOC curve exists, even though the curve differs among batteries. As long as an initial characterization is done through simple experiments, one can use the OCV to determine SOC without complicated model development tasks. Avoiding complex battery modeling lets this method have wider applications. One scenario where the OCV method can be applied is hybrid energy applications. Such an example involving distributed energy generation is shown in [49] which utilizes batteries to match the load demand whether there is a surplus or a shortage in energy generated. Here the OCV method could be applicable if the system has multiple energy storage elements. The major drawback of the OCV-based SOC estimation method is that it requires the battery to be switched off from the circuit for a period of time. Unless the system can allow a parallel battery configuration or allow the battery to be disconnected from the system for a duration, this method would not be suitable without intensive modeling. The other drawback is that the OCV vs. SOC curve varies if the operating temperature changes [50]. Therefore, if the system is subject to large temperature variations, this approach may not be suitable without modification.

In this research, the study investigates the OCV-based SOC estimation approach described above, in conjunction with switching, for lithium ion batteries. The main focus of this study is on lithium ion batteries because they have higher energy storage capability compared to other existing battery technologies [1].

1.3 Basic Operating Principle of Lithium-Ion Battery

The basic elements of batteries are anode, cathode and electrolyte. As a lithium ion battery is charged or discharged, a lithium exchange occurs between anode and cathode owing to ion transport within the electrolyte of the battery. The number of factors of the battery relates to the thermodynamic parameters of the battery such as lithium stoichiometry, which

relates to the state of charge. The basic discharge reaction of a Li-ion battery is shown in Equation (1.2) where CA and AN are the working electrodes [34].

$$Li_xAN + CA \xrightarrow{discharge} AN + Li_xCA \tag{1.2}$$

Fig. 1.1 illustrates the basic operating principle of lithium-ion batteries [1]. For safety reasons, the common commercially available rechargeable Li-ion battery is in its ionic, rather than metallic state. The energy level of the lithium-ion battery varies as the positive and negative electrode materials change. The use of different lithium-ion cathode materials such as $FePO_4$ and structures such as carbon nano-tubes provides ongoing research for the public and private sectors.

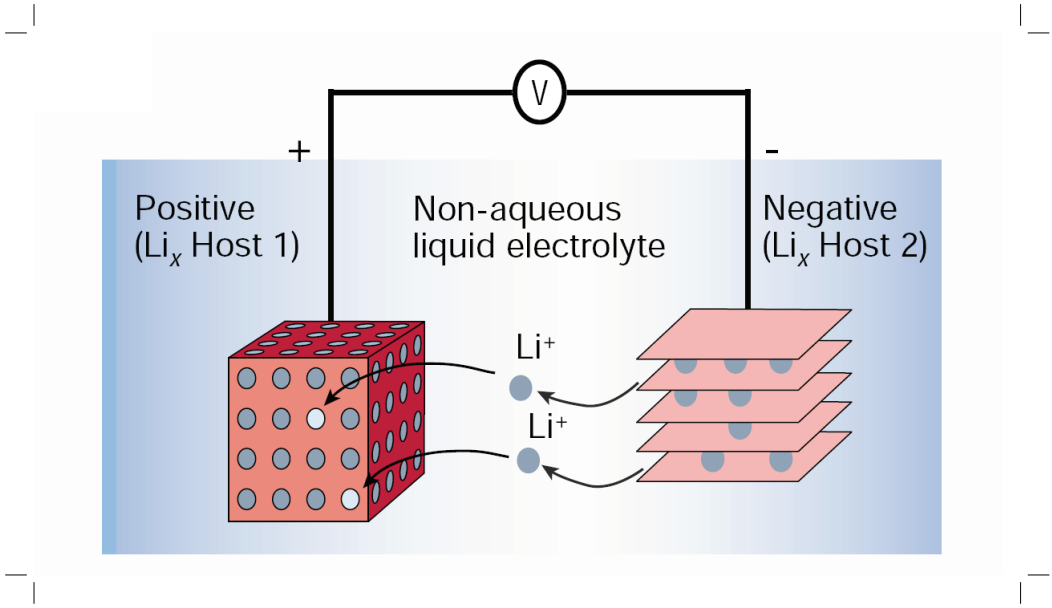

Figure 1.1: Rechargeable Lithium-Ion Battery During Discharge [1]

Lithium ion batteries have many advantages over other types of chemistry such as Nickel-metal hydride or lead acid batteries. Higher energy density, lighter weight, longer cycle life and no memory effect make lithium ion batteries very popular in battery technology advancement among research groups. Lithium ion batteries weigh on average one-third the weight of lead acid and 65% the weight of nickel-metal hydride batteries. This

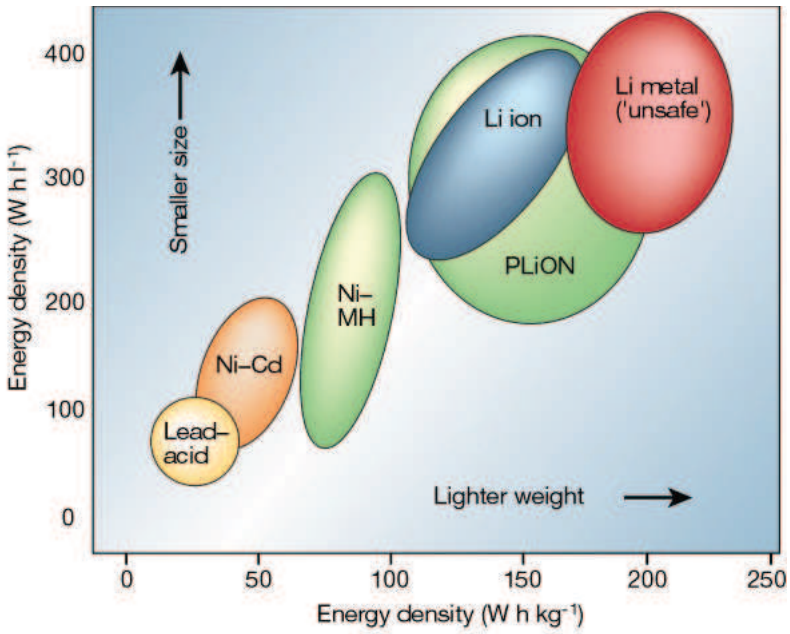

Figure 1.2: Comparison of Battery Technologies in Terms of Volumetric and Gravimetric Energy Density [1]

reveals important reasons why lithium-ion batteries are very attractive in hybrid vehicle applications. Many research groups have investigated different designs and combinations of lithium-ion battery chemistries and various applications utilizing this battery technology. Fig. 1.2 illustrates the energy density comparison between different battery technologies [1].

Researchers have investigated different types of lithium-ion battery cathode chemistry. Lithium manganese oxide (LMO), lithium titanium oxide (LTO), lithium nickel manganese oxide (LiNiMO), lithium cobalt oxide ($LiCoO_2$) and lithium phosphate are several examples of lithium-ion battery cathode compounds [34]. The voltage and capacity profile varies and depends on the battery's chemical structure. Extensive review of various lithium ion rechargeable batteries can be found in [34].

The specific batteries this thesis investigates are the lithium iron magnesium phosphate ($LiFeMgPO_4$) battery manufactured by Valence Technology and lithium iron phosphate

($LiFePO_4$) manufactured by A123 Systems. The $LiFeMgPO_4$ battery is a battery module with four 3.3V cells. This type of battery tends to have a slower electrolyte reaction which reduces the chance of thermal runaway. In addition, the cost of this material is less compared to a compound such as $LiNi_{0.33}Co_{0.33}Mn_{0.33}O_2$ which has a higher capacity. However, these chemical resources are more limited than phosphate [12]. The $LiFePO_4$ battery is a common commercially available single cell 3.3V battery. The benefit of this type of chemistry is that phosphate-based materials are cost effective and more reliable. Further details on the experimental characterization of these batteries will be discussed in the later chapters.

1.4 Objective

The objective of this thesis is, first, to survey the state-of-the-art in battery state-of-charge estimation methods, as done in the literature review presented earlier in this chapter. Further, a switching-based approach to estimate the SOC of Li-ion batteries is proposed. This method relies solely on the voltage characteristic of Li-ion batteries and uses a switch-off duration for direct measurement of OCV. The thesis carries out hardware experiments to verify the validity and effectiveness of the direct OCV-based SOC estimation method using two different batteries: $LiFePO_4$ and $LiFeMgPO_4$. The thesis further investigates the SOC estimation error incurred using the proposed method. The thesis is organized as follows: A detailed lithium ion battery system description is provided in Section 2.1. Sections 2.2 and 2.3 present two common SOC estimation methods. Chapter 3 and Chapter 4 elucidate battery experimental testing results. Section 3.1 describes the hardware set-up of the experiment and Section 3.2 compares the voltage response between lead acid batteries and Li-ion batteries. Chapter 4 shows the charge and discharge test results of two types of batteries. It describes the SOC estimation approach for direct measurement of the OCV. Chapter 5 proposes improved SOC estimation by utilizing a characteristic time constant reflective of the battery's transient response. Battery time constant variation versus aging

is briefly introduced in Section 5.3. Chapter 6 comprises concluding remarks and future work. Additional information is provided in the appendix.

Chapter 2

Lithium-Ion Battery System

2.1 Basic Properties of Lithium-Ion Battery Monitoring System

Lithium-ion battery is a general term that refers to a family of batteries in which the anode chemistry is lithium-based. Different types of Li-ion batteries are distinguished by their cathode chemistry, such as oxide or phosphate. As briefly mentioned in the earlier chapter, various cathode materials have different properties. This thesis will focus on $LiFePO_4$ and $LiFeMgPO_4$ cathode materials to understand the general properties of the common commercially available batteries.

2.1.1 Lithium Iron Phosphate $LiFePO_4$

The lithium iron phosphate batteries cathode materials have been very popular for commercial use, high power applications and military applications. These types of cathode materials have lower cost compared to other types of cathode materials. In addition, these materials are less toxic than Co, Ni, and Mn-based cathode materials [2]. Compared to only Fe-based cathode materials, which have poor ability for lithium removal, $FePO_4$ material has shown much better battery performance. A comparison of different iron-based cathode materials is shown in Fig. 2.1 [2].

The typical chemical reaction of $LiFePO_4$ is shown in Equation (2.1) and illustrated in

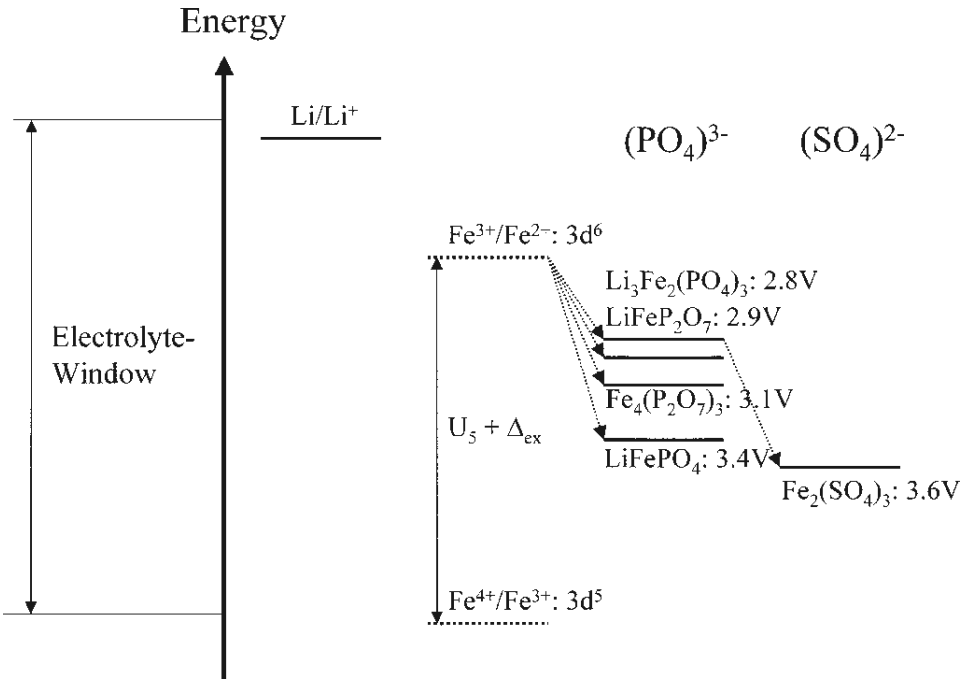

Figure 2.1: Energy Diagram of Some Iron-based Cathode Materials for Lithium ion Batteries [2]

Fig. 2.2 [3].

$$LiFePO_4 <=> FePO_4 + Li + e- \tag{2.1}$$

The $\mathrm{LiFePO_4}$ chemistry has no obvious capacity reduction with several hundred cycles and it has higher stability during charging and discharging [51]. Advantages such as being non-toxic, having thermal and chemical stability and longer cycle life make the iron phosphate a popular battery material in research and applications [2] [52]. One of the disadvantages of this material is that without overdischarge protection, it is easy to damage the cell and diminish its capacity [51]. Therefore, SOC monitoring of this type of cell is critical.

2.1.2 Battery Management System

In order for applications to properly use the battery in their system, a battery monitoring system is a necessity. A battery monitoring system generally includes a means for monitoring the state of charge (SOC) and the state of health (SOH) of the battery. This is for

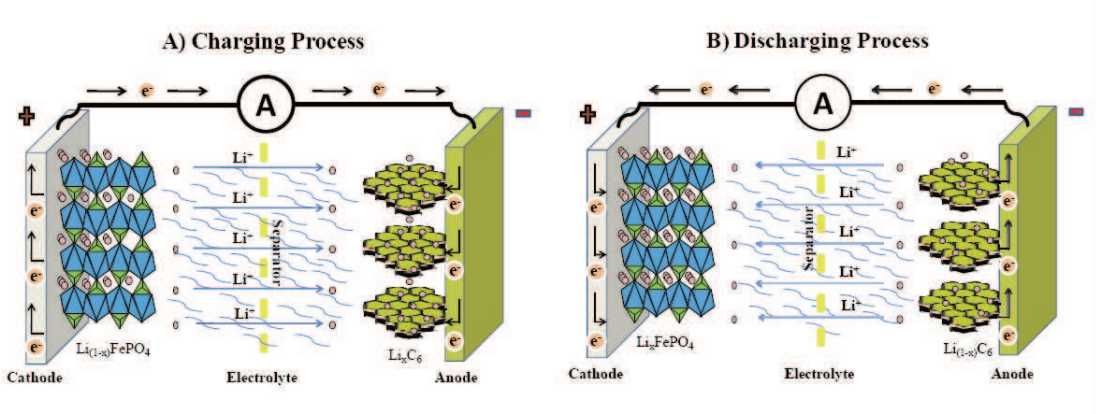

Figure 2.2: Chemical Reaction of $LiFePO_4$ [3]

safety and for application-specific needs. SOC and SOH are critical properties in battery technology and they have been extensively investigated by researchers.

SOC is often defined as the available capacity expressed as a percentage of the current maximum capacity of the cell as shown in Eq.(2.2).

$$SOC = (\frac{Q_{available}}{Q_{rated}}) \times 100\% \tag{2.2}$$

SOH refers to the condition of the battery. It is a common metric for comparing the battery's condition to the battery's performance specifications. SOH typically relates to the age of the battery; SOH generally decreases over time and with use. Equation (2.3) shows the SOH definition. The rated capacity is the battery's capacity when the battery is fresh. The battery total capacity fades over time. It is often recommended to replace the battery if the SOH is below 80%.

$$SOH = (\frac{Capacity_{current}}{Capacity_{rated}}) \times 100\% \tag{2.3}$$

If the SOH is not known, even if the battery is fully charged, it might, for example, only have the effective capacity of 60% of a new cell by comparison. Therefore, SOC, also known as battery's charge content, only indicates the remaining energy in the cell; it does not necessarily indicate the battery's ability to meet the load performance requirement. However, knowing the battery's SOC can prevent overcharging or over-discharging the

battery. SOC indication is often used to prolong battery life, assist battery performance and prevent hazards.

In a battery monitoring system, SOH and SOC are often monitored at the same time by using a different estimation technique. The common properties that are used for SOH and SOC are impedance, capacitance, voltage, self-discharge rate and ability to accept a charge. This thesis is mainly focused on SOC estimation of the battery and it is assumed for a control application, the SOH is at the healthy level.

The knowledge of battery SOC is extremely important for lithium battery applications. An example is automotive applications such as hybrid electric vehicles (HEV) [41]. In order to sufficiently manage the energy used in the HEV and improve fuel efficiency, knowledge of battery SOC is critical in the automotive control system. The battery needs to be able to provide available charging and discharging power to meet the vehicle power requirements.

It is difficult to directly measure SOC without precise laboratory equipment; therefore, various techniques have been developed for SOC estimation. A number of these techniques were discussed in the Introduction, and can be broadly categorized as model-based or model-independent. The two categories are discussed in some more detail in the next two sections.

2.2 Model-Based Battery SOC Estimation

As mentioned in the earlier chapter, model-based battery SOC estimation is commonly used in control systems. The advantage of this method is that the final result can be fairly accurate; however, this method is battery-specific and could even be specific to the type of cathode chemistry. Two types of modeling approaches are often used: the electrochemical model and the equivalent circuit model.

The electrochemical model tends to be more accurate compared to the equivalent circuit model. It takes into consideration the chemical reactions and cell degradation phenomena.

However, without precise laboratory equipment, it is difficult to create an electrochemical model of a battery. This electrochemical model is more complicated and is computationally intensive to execute than the equivalent circuit model.

An example of a Li-ion electrochemical model is given in Fig.2.3 [4]. In this paper, the authors develop a 1D electrochemical cell model coupled with a solid diffusion model. Using this model, chemical properties such as Li+ concentration in solid and electrolyte phases, kinetic and transport properties, etc. can be captured or parameterized. In the work done by [29] and [4], the authors have validated their model by confirming that the open-circuit voltage predicted by the model matched with hardware measurement.

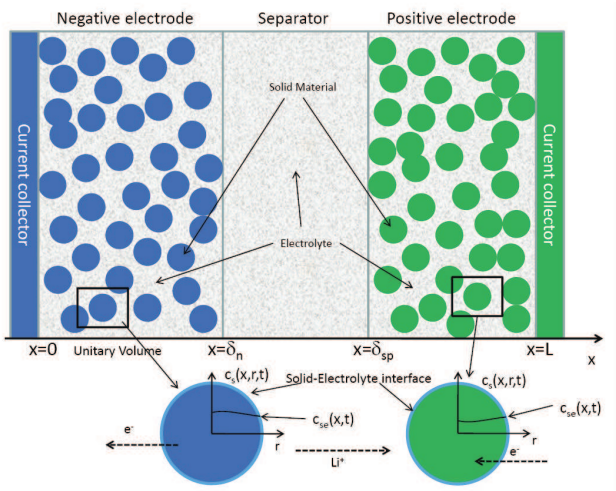

Figure 2.3: Electrochemical Model of a Lithium ion Battery [4]

Fig.2.4 shows an example of the equivalent circuit model. The equivalent circuit model consists of the charge transfer resistance and double layer capacitance. Utilizing this resistance and capacitance, the battery's first order dynamic behavior can be estimated. It can be noted that the SOC estimation is concluded by estimating the OCV. Other equivalent circuit models from the literature also incorporate the diffusion resistance and capacitance into the equivalent circuit. Fig.2.4 shows that the voltage response of the system can be

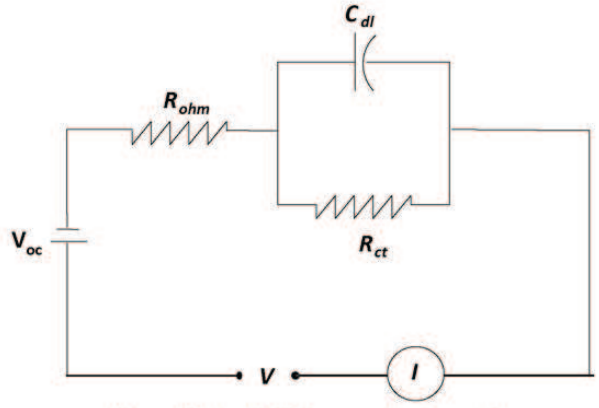

Figure 2.4: Simple Battery Equivalent Circuit Model of a Lithium ion Battery [5]

estimated as the following [5]:

$$V = V_{oc} + IR_{\Omega} + V_{dl} \tag{2.4}$$

where V_{dl} can be calculated using:

$$\frac{dV_{dl}}{dt} + \frac{V_{dl}}{C_{dl}R_{ct}} = \frac{1}{C_{dl}} \tag{2.5}$$

From the modeling approaches that have been followed by several research groups as outlined above, it is observed that models are used to predict the OCV, which is in turn used to measure SOC. However, without using an actual OCV, additional algorithms such as EKF are needed to obtain an accurate SOC result.

2.3 SOC Estimation based on Direct OCV Measurement

Instead of using a modeled-based OCV approach, the SOC can be estimated from a direct measurement of the OCV. If OCV is directly measured then the SOC can be determined from an OCV vs. SOC map of the battery. This approach is simple and inexpensive. Also, using the direct measurement method, modeling is not necessary. However, the true OCV

is only obtained if the battery is switched off (i.e, relaxed) for an infinite duration of time. If the switch-off time is finite, then one measures an approximate OCV and hence incurs errors in the resulting SOC data. Thus, the direct OCV measurement method could be used when voltage relaxation time is allowed.

Directly measuring the OCV to estimate SOC has been attempted for lead acid batteries [53]. The authors discovered that the OCV is affected by the resting time and previous discharged current. Their results show that the estimation error is less than 5% if a resting time greater than 10 minutes is allowed. This is a significant switch-off duration. For Li-ion batteries, experiments show a faster recovery time to its OCV compared to lead-acid batteries [31]. Because of this faster recovery time, the necessary switch-off duration for obtaining a relatively accurate estimate of SOC can be shorter. Hence, this technique could have wider applications for Li-ion batteries. In addition to the property of faster recovery time, Li-ion batteries weigh less (higher power density) than lead acid batteries. A lighter weight battery is advantageous for applications with weight constraints, such as electric vehicle applications, [54]. On the other hand, for Li-ion batteries, the battery's OCV vs. SOC curve is quite flat (low slope) in the 20-80% SOC range. This may lead to higher estimation error even with small errors in OCV measurement. Another disadvantage of direct OCV measurement is that OCV varies with temperature since the capacity of a Lithium cell varies with temperature.

The next few chapters discuss the experiments that were conducted to investigate the direct OCV measurement method for Li-ion batteries and present experimental data to show the effectiveness of this method in estimating SOC.

Chapter 3

Experimental Setup and SOC vs. OCV Characterization

3.1 Experimental Setup

Figure 3.1 [6] shows a snapshot of the $LiFePO_4$ 18650 single cell battery. It is subject to a pulsed current profile using an Arbin BT-2000 battery testing equipment at a constant temperature of $25°C$. The equipment was made available for use for this research by Dr. Brian Landi of the Chemical Engineering department at RIT. The Li-ion cell is charged at a constant current of 1.5A until 3.6V and then held at 3.6V for 45 minutes. The cell is then discharged at 1.1A (i.e, 1C rate). This charging set up follows the recommendations of the data-sheet [6] provided by the manufacturer.

For the $LiFeMgPO_4$ chemistry, a 12V battery module purchased from Valence, Inc. as shown in Fig. 3.2, is used.

Fig. 3.3 depicts a schematic diagram of the experimental setup for testing the battery module. The setup consists of the following equipment:

- A DC 100V/50A programmable power supply from Elgar electronics,
- A dSpace® DS1103PPC controller board,
- Current clampers (sensors) from Fluke,

Figure 3.1: A123 Battery, Figure Courtesy [6]

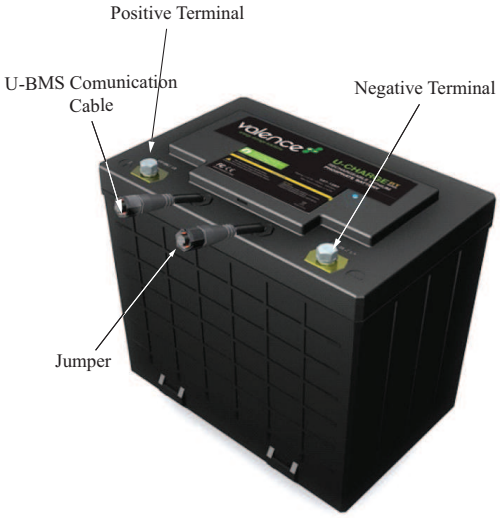

Figure 3.2: Valence, Inc. $LiFeMgPO_4$ 12V Battery Module, [7]

- A DC programmable electronic load from Elgar electronics,
- A voltage divider made from precision resistances for voltage measurement.
- A rated 30A DC relay shown in Fig. 3.5, [8], is used for switching the battery on and off from the circuit.

Fig. 3.4 shows the hardware setup. The dSpace 1103 is a controller board for executing

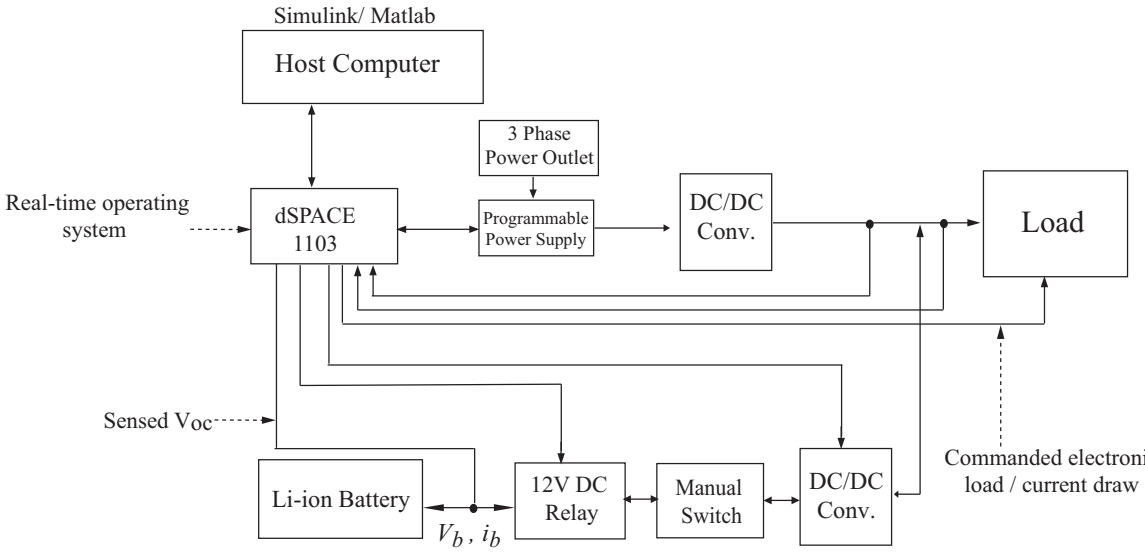

Figure 3.3: Schematic of Battery Module Experiment Setup

real-time simulations. The board has a number of digital-to-analog and analog-to-digital channels for data acquisition, command and actuation. The dSpace controller board and the associated software called ControlDesk® also allow online real-time monitoring. For this work, Matlab® /Simulink® is used for programming the necessary logic, data processing and commands. Utilizing dSpace, Matlab®/Simulink® code is translated into hardware code and executed in real time.

3.2 Lead Acid Battery vs. Lithium Ion Battery

As mentioned earlier, Li-ion batteries have many advantages over other types of batteries. One such advantage is a faster voltage recovery upon switch-off. This implies that for at least some chemistries of Li-ion batteries, upon switch-off the terminal battery voltage approaches the OCV faster than conventional batteries such as lead-acid. In order to compare the recovery times, simple charge and discharge comparison tests are run for a lead acid battery, shown in Fig. 3.6, and a lithium ion battery. Both batteries are 12V modules. A 5A charging/discharge current is applied to the system for the tests. Overall, the test

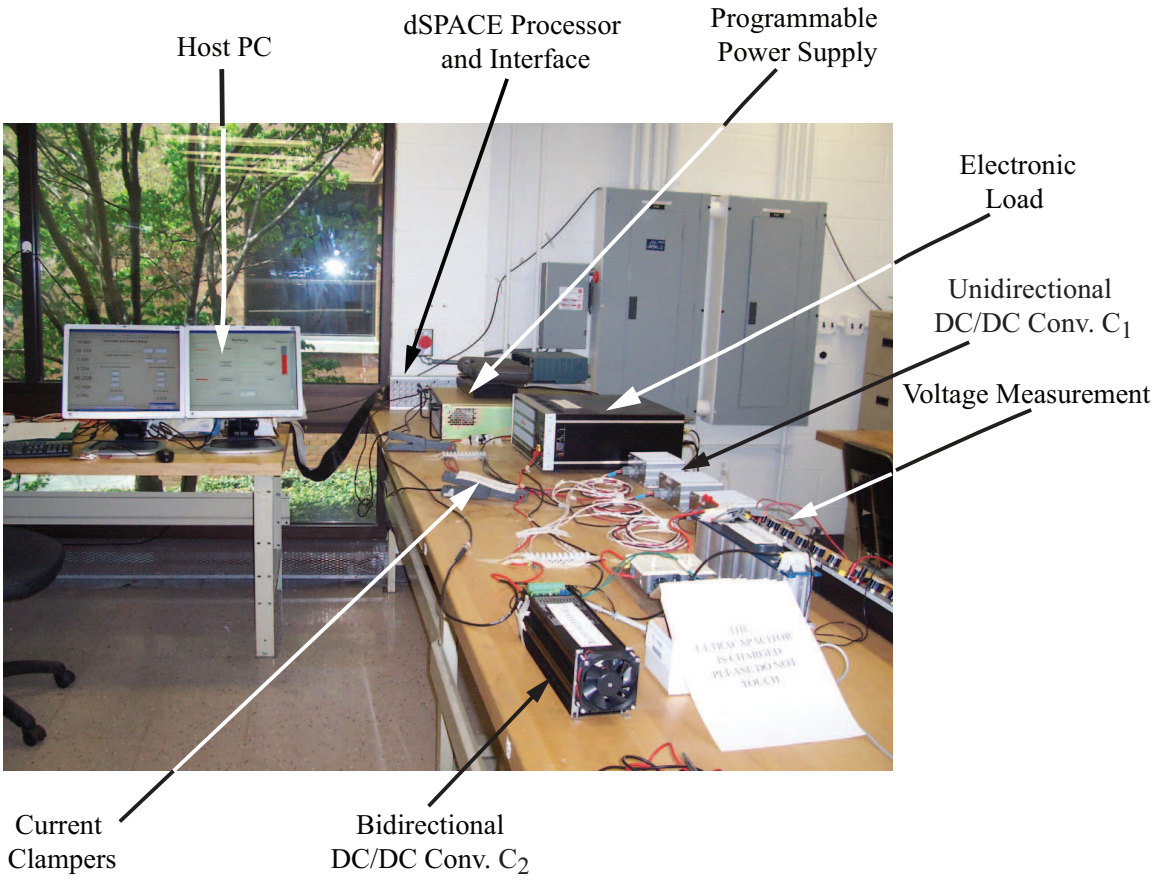

Figure 3.4: Experimental Test Stand Setup

consists of a repeating sequence of pulses with five-minute open-circuit and two-minute charge/discharge.

An NP65-12BFR lead-acid battery module from Energies Inc. is used for this test. For the Li-ion battery, the module shown in Fig. 3.2 is used. The terminal voltage is measured and the comparison results are shown in Fig. 3.7 and Fig. 3.8. It can be seen that during the open-circuit time, the recovery time of the terminal voltage for the lithium ion battery is less than that for the lead acid battery, especially during the charging test. Having a faster recovery time to the open-circuit voltage is advantageous since it is undesirable to switch the battery off from the system for an extended period of time for sensing/estimation purposes.

Figure 3.5: 12 VDC Coil 30A Relay, Figure Courtesy [8]

Figure 3.6: NP65-12BFR Lead-acid Battery Module from Energies, Inc

Because of the faster recovery time, Li-ion batteries are more suitable to utilize the open-circuit voltage method compared to lead acid batteries. The following sections investigate the SOC estimation approach through switching and OCV measurement.

3.3 SOC vs. OCV Characteristics

This thesis uses a switching-based method for SOC estimation. The method works by providing a switch-off interval during which the terminal voltage is measured. The measurement at the end of this interval provides an estimate of the OCV. Subsequently, the

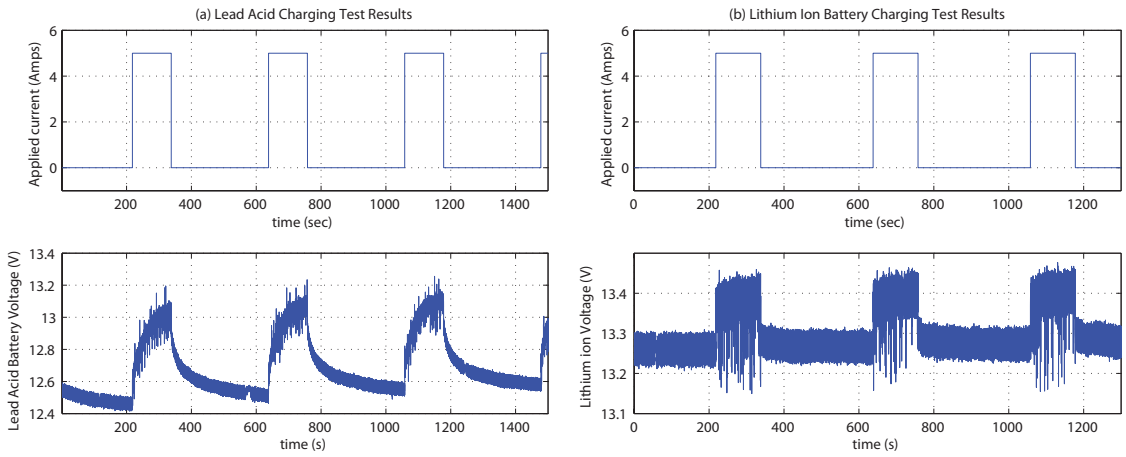

Figure 3.7: Lithium Ion and Lead Acid 5A Charging Data Comparison. (a) Lead Acid battery, (b) Lithium Ion Battery

battery's characteristic OCV vs. SOC plot is used to estimate the SOC. The goal is to understand the accuracy of this method, which is proposed to require a comprehensive battery model. If an error-bound is determined, this method can be incorporated into a robust control system that handles this error and delivers the control objectives of the system in the presence of this error.

In order to use the direct OCV measurement method to estimate SOC, as mentioned above, an OCV vs. SOC curve is needed. The OCV vs. SOC curve can be generated by fully charging the battery and cycling the battery over time.

3.3.1 SOC vs. OCV Curve of $LiFeMgPO_4$ Battery Module

In the preliminary testing of the Valence Technology's U24-12RT Li-ion battery, shown in Fig. 3.2, a diagnostic tool-kit that provides SOC data is used. The tool-kit is shown in Fig. 3.9. The tool-kit can provide SOC data of the battery at any time by using the coulomb counting method in conjunction with a precise model, according to the manufacturer's data [55]. The tool-kit shows consistency when measuring the SOC, which further confirms the accuracy of their monitoring kit. The monitoring tool-kit is used to generate the OCV vs.

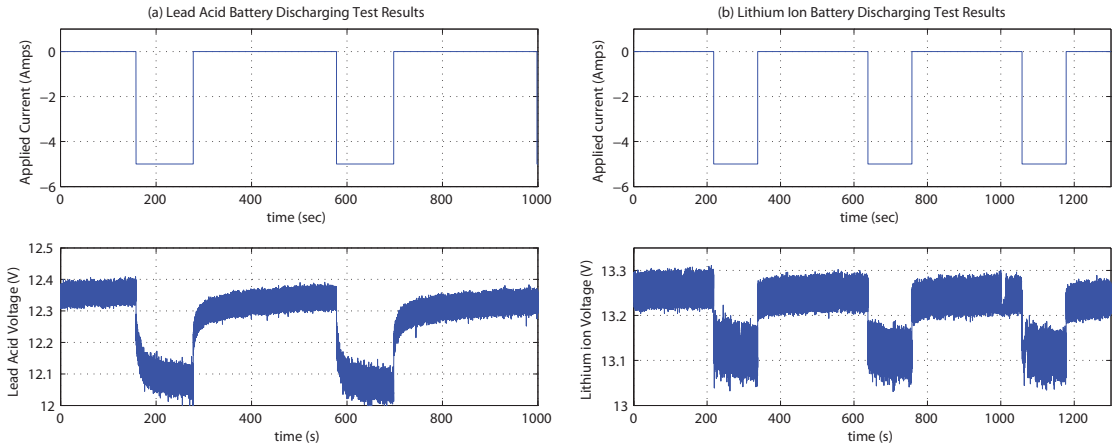

Figure 3.8: Lithium Ion and Lead Acid 5A Discharging Data Comparison. (a) Lead Acid Battery, (b) Lithium Ion Battery

SOC curve of this battery module.

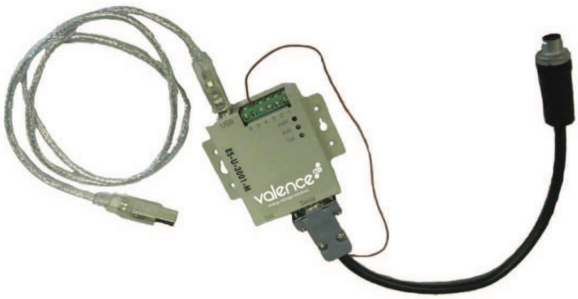

Figure 3.9: Diagnostics Tool-Kit for SOC Measurements of the Valence Lithium-ion Battery [7].

In order to determine the required resting time for accurate SOC estimation, the battery needs to be in quasi-equilibrium status. Preliminary testing is required to determine the quasi-equilibrium point. Fig. 3.10 shows two cycles of the initial test. It can be seen from Fig. 3.10 (a) and (b) that within the first 100 seconds, the voltage slowly converges to an equilibrium. It is safe to assume that after five minutes of switch-off time, the open-circuit voltage reading has minimal change from observation.

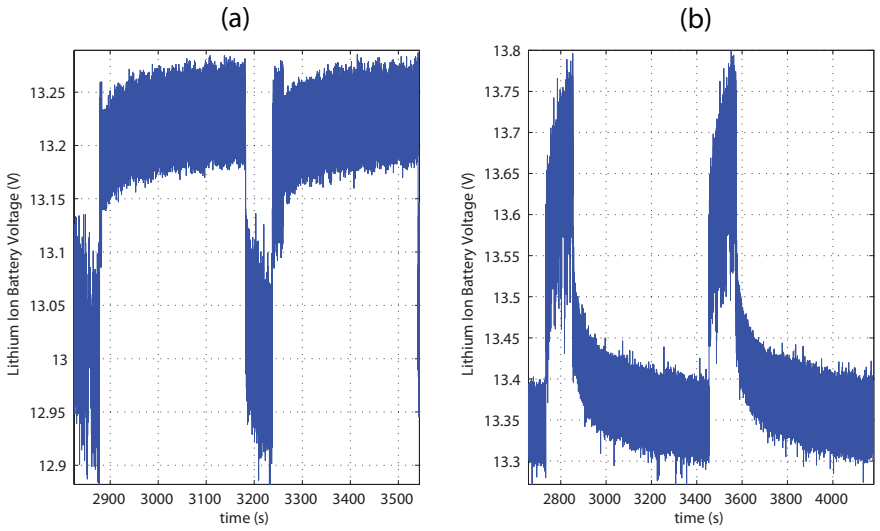

Figure 3.10: (a)20A Discharging Plot,(b)20A Charging Plot

From Fig. 3.10, it is noted that the transient time of charging the battery is longer than discharging the battery. The charging and discharging measurements of the SOC have variations depending on how long the wait time is. As predicted, the longer the rest time, the more accurate the SOC result.

The OCV vs. SOC curve generated for this battery is shown in Fig. 3.11. The plot is generated by charging the battery from 0% SOC to 100% SOC and discharging from 100% to 0%. This test uses 20A current for charging and discharging the battery. During the charging or discharge, the SOC as displayed by the battery management system is monitored. At approximately 1% intervals of SOC, the battery is switched off and the open-circuit voltage is recorded after five minutes of switch-off time. This experiment uses the tool-kit shown in Fig. 3.9 to record the SOC provided by the in-built battery monitoring system.

It is noted that slopes of the curve between 10% and 95% SOC are flatter than above 95% or below 10%. Also, note that with the proposed switching approach, the error of SOC estimation would be lower as the slope of the OCV vs. SOC curve increases. Therefore, the open-circuit voltage method is more accurate when the SOC is below 10% or above 95%. This behavior has been observed by [56], where the authors stated that there is a

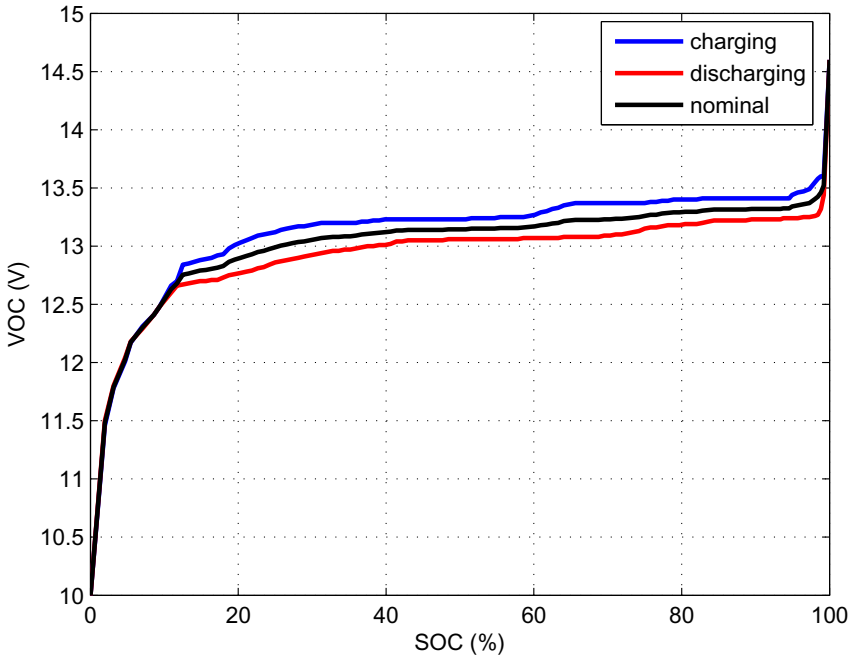

Figure 3.11: V_{OC} vs. SOC of Lithium iron Magnesium Phosphate Battery Module

limitation of the usefulness of the mid-SOC range because of its small slope. Nevertheless, as mentioned in the earlier section, the state of charge estimation is important for battery protection and safety concerns. A SOC measurement is used for preventing a battery from being overcharged or overdischarged. Moreover, the SOC of the battery would typically lie in the mid-SOC range for a majority of the battery's operating time. Hence, it is important to investigate the accuracy with which the SOC can be estimated, even when in the mid-SOC range.

3.3.2 SOC vs. OCV Curve of $\mathrm{LiFePO_4}$ Single Cell Battery

When generating the OCV vs. SOC curve during the preliminary testing of the $LiFePO_4$ single cell battery, the battery is charged at a constant current of 1.5A until 3.6V is reached, and then held at 3.6V for 45 minutes. The cell is then discharged at 1.1A or 1C rate. The charge data and total capacity is provided by the Arbin BT-2000 cycler. The SOC is

determined by using Equation (2.2). The OCV vs. SOC curve of the single cell battery is shown in Fig. 3.12.

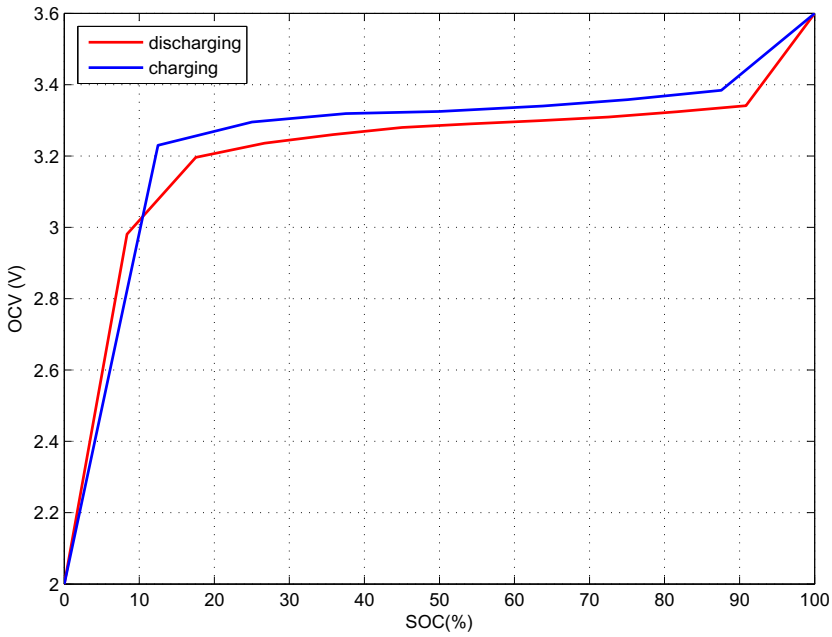

Figure 3.12: V_{OC} vs. SOC of Lithium iron Phosphate Single Cell Battery

Compared to the 12V battery module whose OCV vs. SOC curve is shown in Fig. 3.11, it can be seen that the single cell battery has similar behavior for the OCV. The slopes of the curve between 10% and 90% SOC are flatter than above 90% or below 10%.

3.3.3 Battery Hysteresis Effect

Both $LiFePO_4$ and $LiFeMgPO_4$ OCV vs. SOC plots show a difference between charging and discharging cycles. There is roughly a 200mV difference for the battery module, and 20mV difference for the single cell battery between the charging and discharging plots. This behavior has also been observed in [47] and [9]. It is referred to in the literature as the hysteresis effect, and a detailed explanation is given in [9].

In [9], the authors explain that the charging electrode particles carry higher voltages

than discharging electrode particles, so the hysteresis between charged and discharged voltage does not disappear as the charging/discharging current vanishes. The occurrence of this behavior is because the time constant related to the charge transfer between charging and discharging batteries is different. The chemical reaction time of the battery cell varies between charging and discharging. There are delays between the battery potential and its chemical reaction. Energy is lost during the charge/discharge cycle because of hysteresis effects. Fig. 3.13 from [9] illustrates the hysteresis effects of a $LiFePO_4$ battery experimental data.

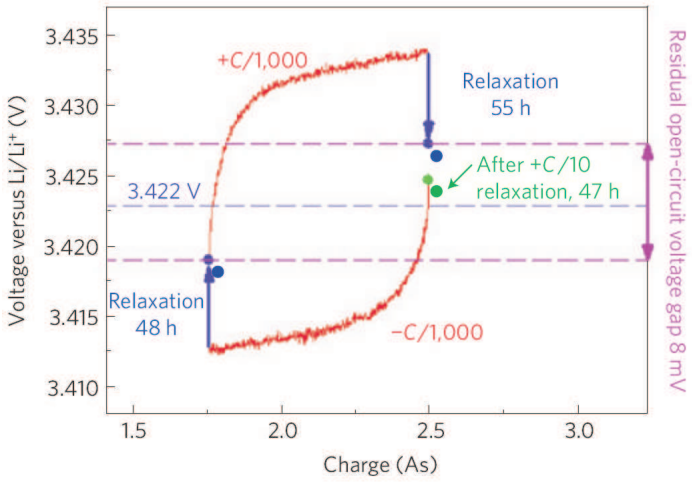

Figure 3.13: Equilibrium Behavior of $LiFePO_4$ Battery [9]

An explanation for this hysteresis phenomenon is related to heat dissipation. During the charge/discharge process, most systems show a positive heat value within a limited compositional range, resulting in a plateau-shaped potential profile. As the temperature rises, the chemical conversion process rate increases, resulting in a change in voltage potential. This clarifies why the hysteresis decreases as the rate of charging and discharging decreases.

Using the knowledge of the battery's hysteresis property and the OCV versus SOC curve from a constant operational temperature, the next step of this research is to investigate the accuracy of the direct open-circuit voltage measurement between different switch-off times.

As the battery switch-off time is increased, the estimation error is expected to decrease. Investigating the relationship between the switch-off time and amount of estimation error is the goal for the next section. The charging, discharging and nominal OCV versus SOC curve are applied for initial simulation for SOC estimation.

Chapter 4

Switching-Based SOC Estimation

4.1 Application to $LiFeMgPO_4$ Battery Module

The battery characterization test uses DSpace and Matlab® to analyze data. This experiment uses the SOC monitoring software available within the battery management system to verify the SOC estimated through switching. It is assumed that the SOC data provided by the software is more accurate than the estimate that will be obtained from direct OCV measurement in conjunction with the OCV vs. SOC curve of the module given in Fig. 3.11. From the data gathered from Fig. 3.11, two curves are applied to the charging and discharging tests. Fig. 4.1 shows the charging test: a 20A current is applied to the battery module, and it is charged for two minutes. Thereafter, the circuit is opened for five minutes. This sequence is repeated from 0% SOC to 100% SOC. A third-order Butterworth filter is used to filter noise in the voltage measurement. Fig. 4.2(a) shows a section of resulting SOC estimate generated after applying the terminal voltage data to the OCV vs. SOC charging curve. Fig. 4.2 (b) instead presents the SOC estimates generated from the nominal OCV vs. SOC curve from Fig. 3.11. The two plots are given to show the difference between the battery management system-generated SOC and the switching-based SOC estimates obtained using first the charging OCV vs. SOC plot and then the nominal (average) OCV vs. SOC plot. It must be noted that in these plots, the relevant SOC data corresponds to the intervals when the battery is switched off (i.e, when the battery current is zero).

Fig. 4.3 and Fig. 4.4 display results from the discharge test. The battery is discharged

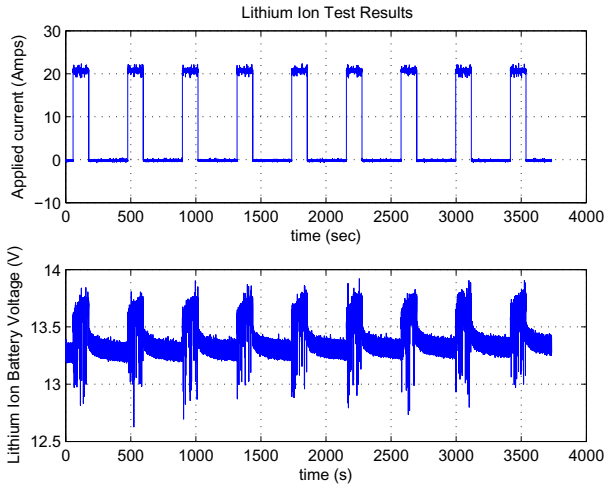

Figure 4.1: 20A Charging Test

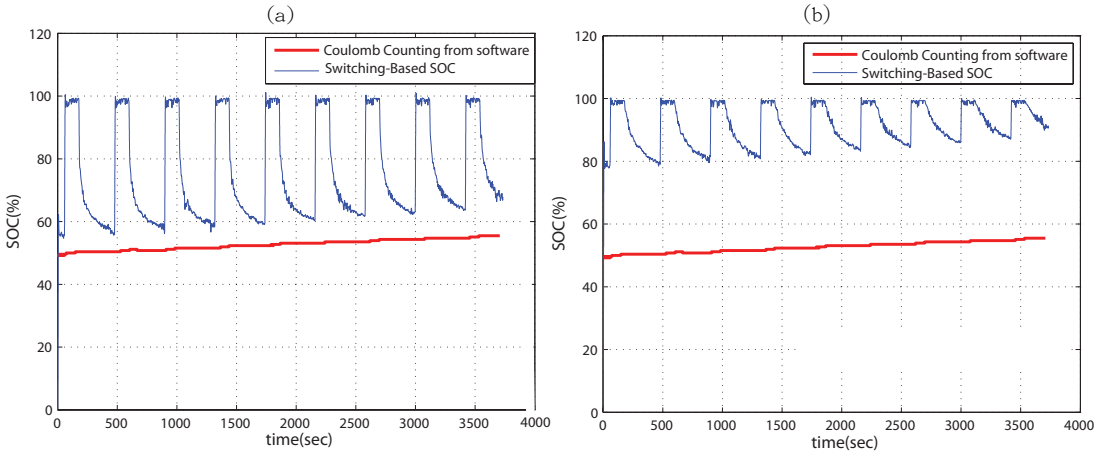

Figure 4.2: SOC Comparison (a)SOC Data Obtained from Charging OCV vs. SOC Curve, Fig. 3.11 (b) SOC Data Obtained from Nominal OCV vs. SOC Curve, Fig. 3.11

for two minutes and switched off (i.e, open-circuit) for five minutes. This sequence is repeated several times. The plot in Fig. 4.4(a) uses the discharging OCV vs. SOC curve of Fig. 3.11 for estimating the SOC and Fig. 4.4(b) uses the nominal OCV vs. SOC curve of Fig. 3.11.

From the results shown in Fig. 4.2 and Fig. 4.4, we next determine an estimate of the magnitude of error observed after a 30 second switch-off time. Zoomed-in views into the 20A charging and discharging plots of Figs. 4.2 and 4.4, are shown in Fig. 4.5.

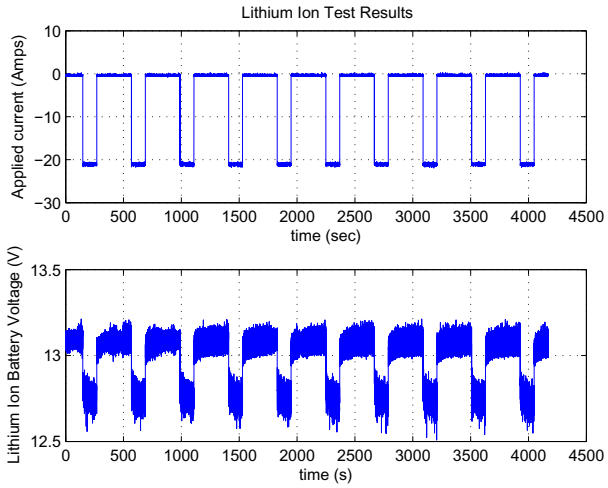

Figure 4.3: 20A Discharging Test

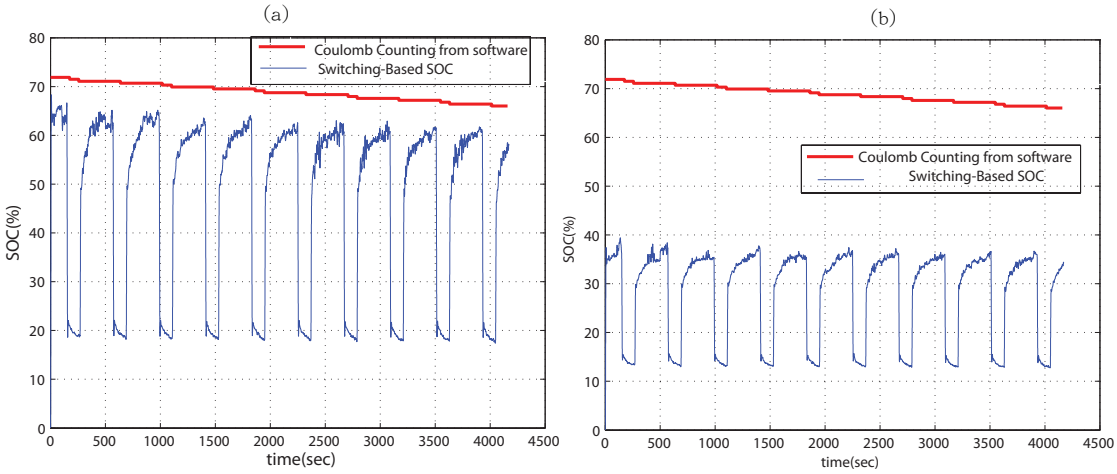

Figure 4.4: SOC Comparison (a)SOC Data Obtained from Discharging OCV vs. SOC Curve, Fig. 3.11 (b) SOC Data Obtained from Nominal OCV vs. SOC Curve, Fig. 3.11

Both charging and discharging results indicate the maximum SOC estimation error due to a 30 second switch-off time is within 15% if the proper OCV vs. SOC curve is applied. The transient time for charging the battery is longer than discharging the battery. From the test results, it shows that for the highest rated charge/discharge current (20A in this case), when the SOC is around 50%, the error is within approximately a 15% boundary.

In order to verify the assumption that higher charging and discharging current causes higher error, Figs. 4.6 and 4.7 present 5A charging/discharging tests with the same testing

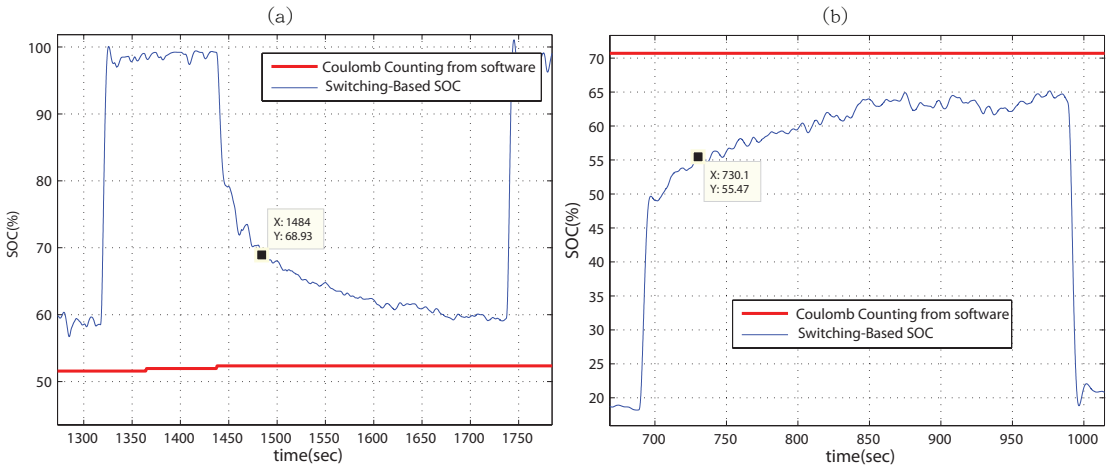

Figure 4.5: (a)Zoomed in 20A Charging Plot Using the V_{OC} vs. SOC Charging Curve, (b)Zoomed in 20A Discharging Plot Using the V_{OC} vs. SOC Discharging Curve.

time period (five minutes open-circuit time and two minutes charging or discharging time). The 5A charging and discharging tests follow the same pattern as the 20A results. For charging tests, plotting against the charging OCV vs. SOC curve has a better fit than plotting against the nominal curve. For discharging tests, the discharging OCV vs. SOC curve has a better fit than the nominal curve. Comparing the 5A and 20A results, the 5A results have errors less than 10% for the charging test and less than 5% for the discharging test. As observed for the 20A case, the transient of the terminal voltage is slower during the charging cycles than the discharge cycles. A general observation is that the time it takes for the terminal voltage to reach equilibrium is longer for a battery that was previously charged than discharged.

The method mentioned above with our battery can be incorporated in control applications, such as distributed energy systems, which can be robust to a 15% error in battery SOC estimate. It is important to stress that when the SOC goes below 10% and above 90%, the SOC estimation error would drastically decrease due to the sharp slopes in OCV vs. SOC curve. Prevention of overcharging and over-discharging of the battery can be achieved relatively easily as the sharp changes in the OCV would be more readily observable than in the mid-region of the OCV vs. SOC curves.

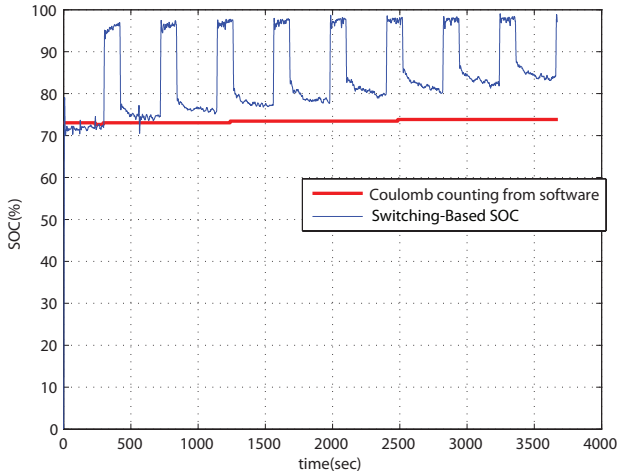

Figure 4.6: 5A Charging SOC Data from Charging Curve

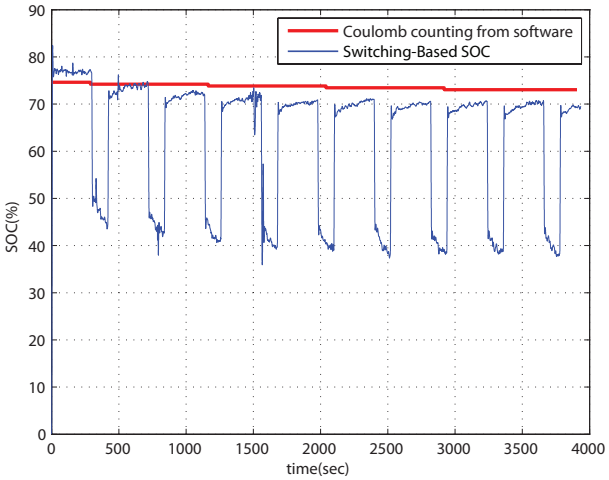

Figure 4.7: 5A Discharging SOC Data from Discharging Curve

4.2 Application to A123 $LiFePO_4$ Cell

A test of two minutes open-circuit voltage and five minutes of charging from 0% to 100% and discharging from 100% to 0% is performed for the single cell battery. Based on the recommendation from the battery datasheet, the charging current and discharging currents for this test are 1.5A and 1A, respectively. Fig. 4.8 shows one cycle of the battery charging and discharging test. Over 500 cycles are performed to confirm repeatability for the SOC

estimation method in this thesis. The single cell battery's energy density is lower than that of the battery module. The time it takes to fully charge and discharge the battery is much shorter compared to the battery module tested in the previous section.

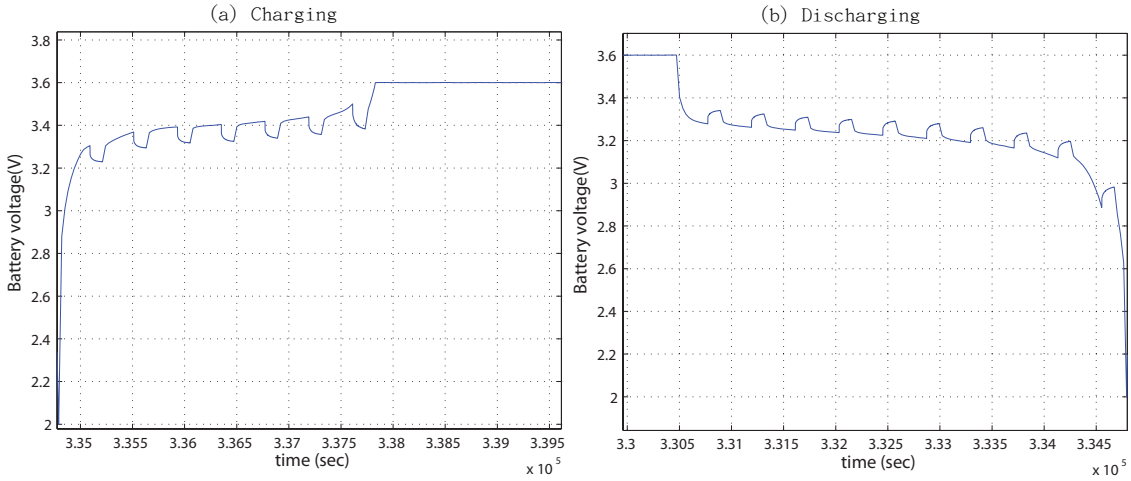

Figure 4.8: A123 LiFePO4 Battery (a) Charging and (b) Discharging Test

The SOC estimation results are shown in Fig. 4.9 and Fig. 4.10. Note that the actual SOC plot (in red) must be compared to the estimated SOC (in blue) only during switch-off duration. The switch-off durations can be seen as the durations when the estimated SOC approaches close to the true SOC. It can be seen that the discharging plot has a lower error value for the same time frame. At the end of two minutes, when the battery is charging, the maximum estimation error is roughly 10%. When the battery is discharging, the error is minimal; this indicates that the battery is reaching its equilibrium point much faster after discharging than after charging. Fig. 4.11 illustrates the zoomed-in plot of Fig. 4.10. There is approximately a 2 % error at the end of the two minutes of battery switch-off time. The average error of estimation is approximately at 2 %. The results shown in this section are similar to those of the 12V battery module tests. The direct OCV measurement method has less error during discharging than charging. It is apparent that if the battery's operating mode (i.e, charging or discharging) immediately prior to a switch-off is known, then one can predict if the magnitude of error will be relatively larger or smaller.

The results for the repeatability test, which investigates the accuracy of switching-based

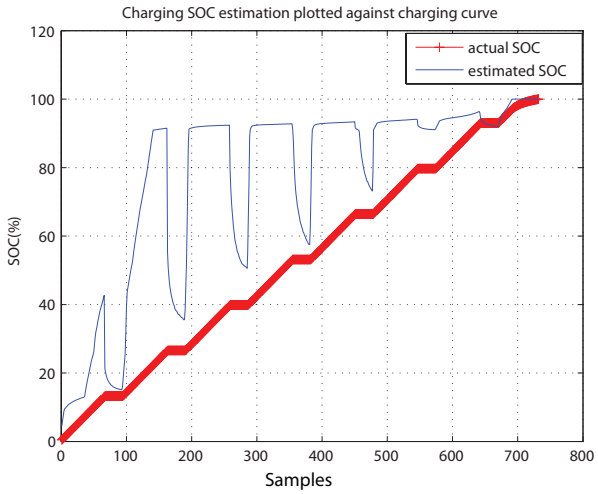

Figure 4.9: A123 Battery Charging SOC Data from Charging Curve

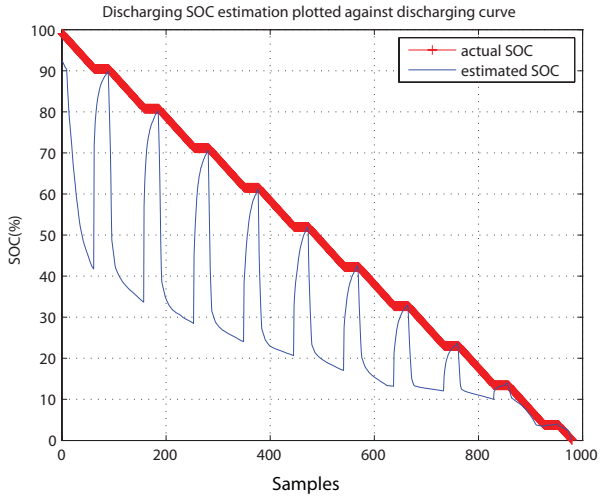

Figure 4.10: A123 Battery Discharging SOC Data from Discharging Curve

SOC estimation over a period of hundreds of cycles, can be seen in Fig. 4.12. Here, the transients are plotted at the 20th discharge cycle and 441st discharge cycle. There is a slight difference between cycle 20 and cycle 441; it is less than 1% error difference. Thus, it gives an indication that for the Li-ion chemistry considered, the effect of aging on the switching-based SOC estimation method is potentially minimal and is almost negligible for a range of about 500 cycles.

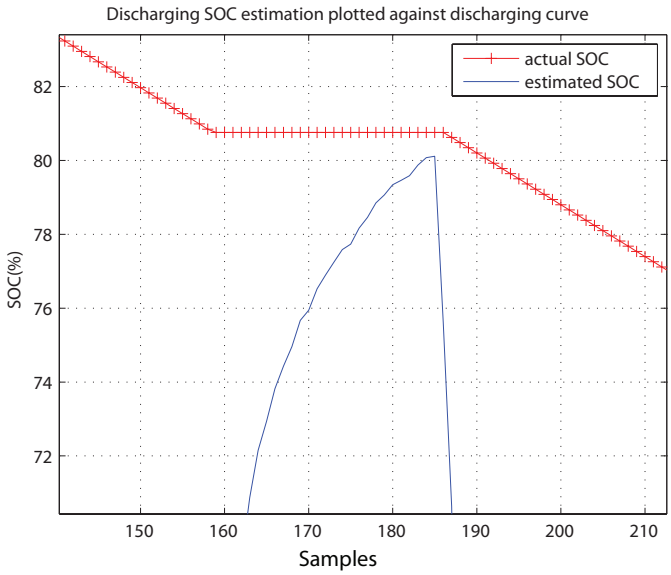

Figure 4.11: Zoomed in A123 Battery Discharging SOC Data from Discharging Curve

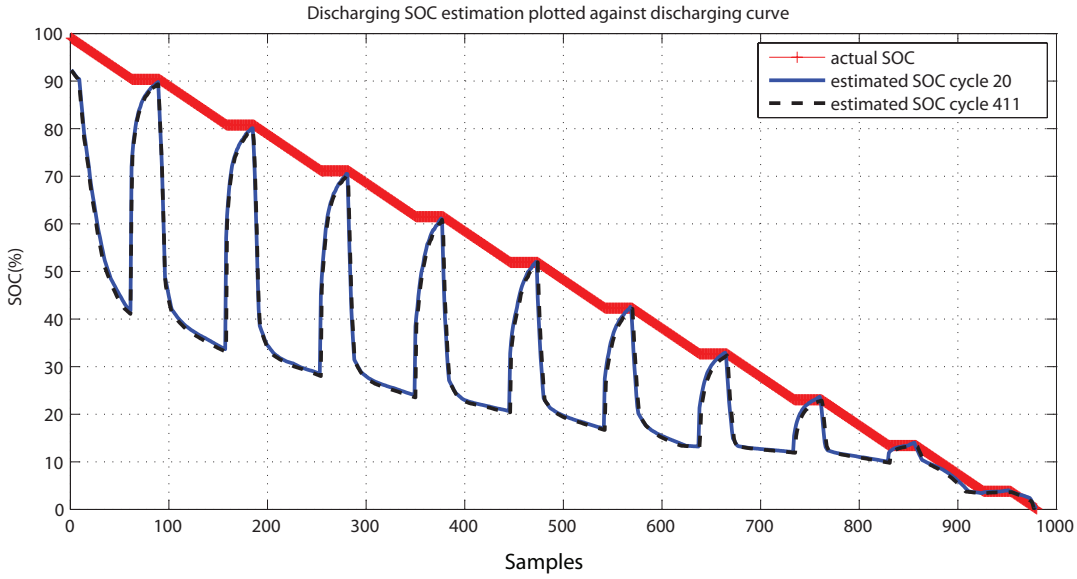

Figure 4.12: A123 Battery Fresh and Aged Battery Comparison

Chapter 5

SOC Estimation using Battery Transient Characteristics

5.1 Time Constant from Battery Transient Response

The data of Chapter 4 shows estimation error of OCV measurement as around 15% for a battery module and 10% for a single cell battery given a two minute switch-off time. While practically usable, an error of up to 15% is highly undesirable, and as such should be minimized. To that end, characteristics of the instantaneous state of charge curve can be identified to aid in both accuracy and convergence time of OCV-based SOC measurement. Examining the SOC curve of Fig. 5.1, observations are noted of some characteristics regarding the transient behavior of the curve as the device under test is disconnected. First, the transient voltage recovery of the battery during switch-off is composed of two different components. An initial fast response with almost instantaneous jump in voltage is followed by a second exponential transient with a larger time constant. Measurements taken after the fast transient and identifying the time constant of the second transient response, resulted in a better agreement of the estimated SOC with actual value. Convergence time is thus lowered by identifying the underlying behavior of the slow transient from a short series of measurements. Accuracy may be improved by evaluating the slow transient for a larger monitoring time, providing a better estimate of the time constant, [57].

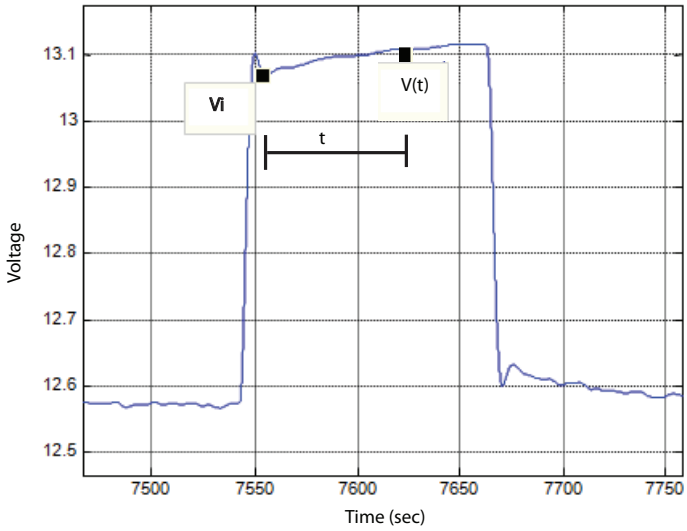

Figure 5.1: Initial Value of Slow Transient Section

A first-order model is assumed for the slow transient and accordingly Equation 5.1 is used to calculate the time constant from the terminal voltage data.

$$V(t) = V_i e^{\frac{-t}{\tau}} + V_f(1 - e^{\frac{-t}{\tau}}) \tag{5.1}$$

In the equation above, V_i is the initial voltage at the beginning of the slow transient, $V(t)$ is the voltage at any interval t during the transient after V_i, V_f is the steady-state voltage (OCV), and τ is the time-constant. Calculation of V_f is completed by rearranging Equation (5.1) which yields

$$V_f = \frac{V(t) - V_i e^{\frac{-t}{\tau}}}{1 - e^{\frac{-t}{\tau}}} \tag{5.2}$$

To calculate the time constant, the terminal voltages at two separate instants of time are used in conjunction with Equation 5.2. Let the two instants be denoted by t_1 and t_2 where the terminal voltages are $V(t_1)$ and $V(t_2)$. Then since the steady-state voltage V_f is same for one transient response, i.e, for both instants t_1 and t_2, from Equation 5.2,

$$\frac{V(t_1) - V_i e^{\frac{-t_1}{\tau}}}{1 - e^{\frac{-t_1}{\tau}}} = \frac{V(t_2) - V_i e^{\frac{-t_2}{\tau}}}{1 - e^{\frac{-t_2}{\tau}}} \tag{5.3}$$

The above equation is solved to determine the value of the time constant τ of the slow transient during switch-off period.

5.1.1 Time Constant of the $LiFeMgPO_4$ Battery Module

The switch-off and terminal voltage measurements for time constant calculation are set up with a two minute switch-off time interval and a five minute charge/discharge time interval with continuous measurement from 0% SOC to 100% SOC. Although there is an effect of sensor noise, a continuous measurement spanning the entire 0% SOC to 100% SOC is done to generate more reliable data rather than fragmented experiments conducted over several sub-ranges of SOC.

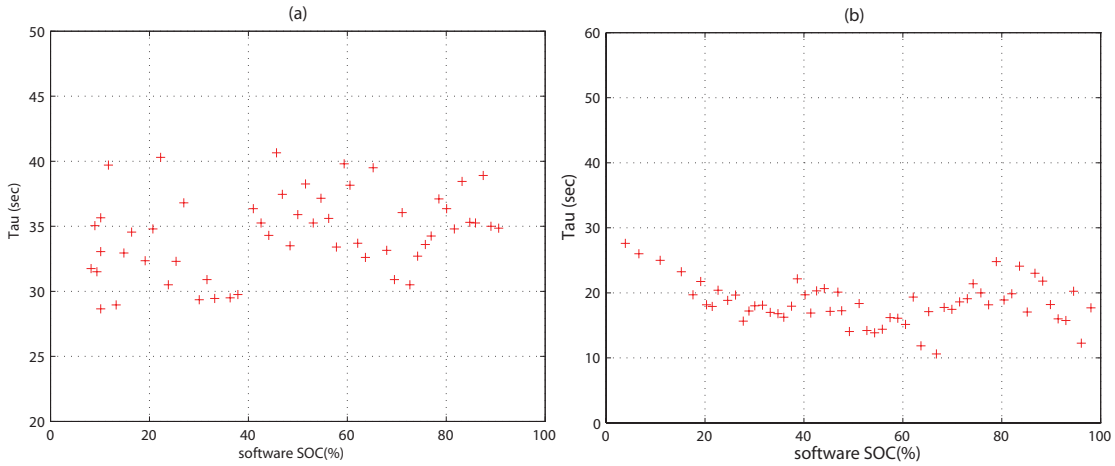

Figure 5.2: (a) Charging Time Constant, (b) Discharging Time Constant

Fig. 5.2 shows that the time constant stays relatively uniform during both charging and discharging tests. The time constant during charging is slightly larger compared to the discharging test. Chapter 3 shows that the transients in discharging cycle have a faster recovery time than those in charging cycles, and Fig. 5.2 confirms this observation. The hysteresis effect, discussed in Section 3.3.3, impacts the time constant between charging and discharging. Note also that the data of Fig. 5.2 confirms there is no significant variation of the time constant over the 0% SOC to 100% SOC range in both charging as well as

discharging cycles. A single τ can be chosen to simplify the SOC estimation and minimize the OCV estimation error.

5.1.2 Time Constant of the $LiFePO_4$ Single Cell Battery

The same experimental system with an Arbin BT-2000 is used to calculate the time constant for the slow transient of the $LiFePO_4$ single cell battery. The switch-off time is a two minute interval followed by a charge/discharge time interval of five minutes. Equation (5.1) is used to calculate the time constant. The process is essentially the same as that of the battery module time constant calculation. The results are shown in Fig. 5.3. The results are plotted against cycle numbers to study variations associated with aging of the battery. For the charging test, there appears to be an increase in time constant as the SOC increases. For the discharging test, there is also a general trend of increasing of time constant as the SOC increases. The increase in time constant over the entire SOC domain is around 7 seconds. However, from the cycles, it can be observed that during discharge at lower SOC values, the time constant can vary up to 10 seconds. This can be an indication of battery's health, which is investigated further in this chapter.

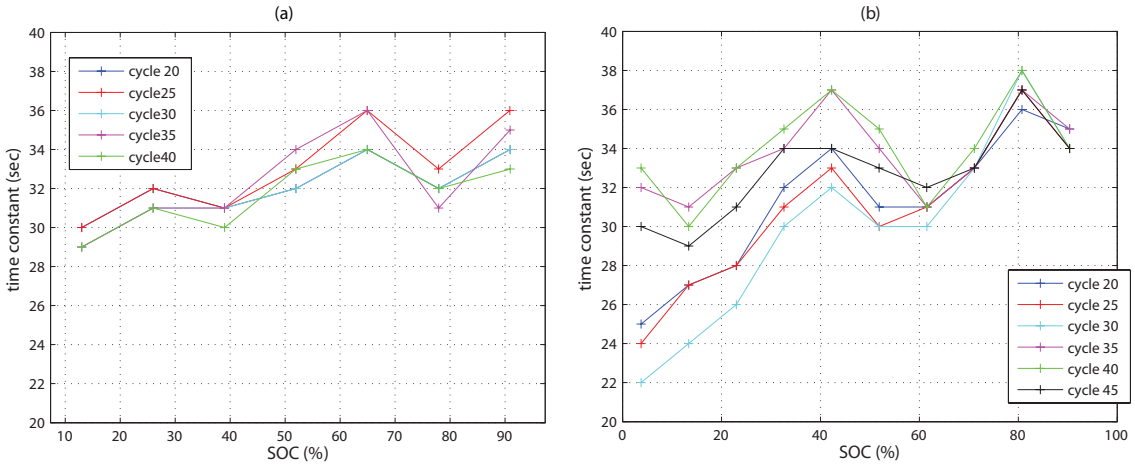

Figure 5.3: Single Cell Battery Time Constant Calculation (a) Charging Time Constant, (b) Discharging Time Constant.

As before, a single τ value will be used rather than a variable quantity to simplify the

resulting SOC estimation method. The next section shows the improved SOC estimation results for both the battery module and the single cell battery.

5.2 SOC Estimation using Switch-off combined with Time Constant

A single time constant is used to keep the estimation method simple instead of using a different time constant for each SOC. Taking the average of the time constant calculated in Section 5.1, the results in Fig. 5.4 , Fig. 5.5 , Fig. 5.6 and Fig. 5.7 are generated with 30 seconds switch-off time. The plots illustrate the contrast between the estimated SOC and the actual SOC obtained from the software of the battery management system. The average time constant of charging and discharging for the $LiFeMgPO_4$ battery is 35 seconds and 18 seconds, respectively. The average time constant for the single cell $LiFePO_4$ battery is 32 seconds and 33 seconds for charging and discharging, respectively. The summary of the result is shown in Table 5.1. The maximum error of the $LiFeMgPO_4$ is over 10% and over 5% for the $LiFePO_4$ battery. In order to reduce this error, an optimal value τ is chosen as the value to minimize the RMS deviation of the predicted SOC from the actual SOC. Equation (5.4) is used to calculate the RMS error. Root mean square deviation (RMSD) is commonly used to measure the differences between predicted values and the actual observed values.

$$|e| = \sqrt{\frac{\sum_{i=1}^{N} e_i^2}{N}} \tag{5.4}$$

Fig. 5.8 displays the resulting RMSD for charging and discharging cycles for the 12V $LiFeMgPO_4$ battery module. The comparison uses the data from the cycling time of two minutes open-circuit voltage and five minutes charging and discharging time. Minimal errors are obtained at 44 seconds during the charging test and 28 seconds during the discharging test. Thus, the single time constant is chosen to be 44 seconds and 28 seconds when the battery is charging and discharging, respectively. The time constants are in the

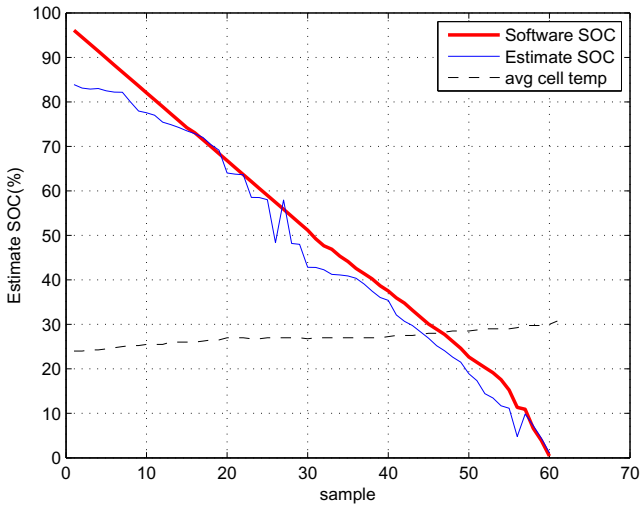

Figure 5.4: 30 Second Switch-off Time for SOC Estimation When Battery is Discharging with Average Time Constant of 18 Second

Table 5.1: Battery SOC Estimation Result

Battery Test	Max Error (%)	Min Error (%)	Mean Error (%)	Switch-off time (sec)
Battery Module Charging (τ=35)	10.34	0.02	3.64	30
Battery Module Discharging (τ=18)	12.21	0.03	3.96	30
Single Cell Charging (τ=32)	3.66	0.03	1.57	30
Single Cell Discharging (τ=33)	5.31	1.29	3.31	30

range of the individually calculated time constants shown in Fig. 5.2. Fig. 5.9, Fig. 5.10, Fig. 5.11, and Fig. 5.12 are generated using the chosen time constant of 44 seconds and 28 seconds. To compare, switch-off times of 30 second and 60 second are used. The plots illustrate the contrast between the estimated SOC and the actual SOC obtained from the software of the battery management system. Fig. 5.9 and Fig. 5.10 are the charging and discharging SOC plot of a 60 second switch-off time. Fig. 5.11 and Fig. 5.12 are the plots of a 30 second switch-off time.

The SOC estimation errors are summarized in Table 5.2. Both charging and discharging tests show minimal improvement by waiting an additional 30 seconds. Using the time constant to estimate SOC can reduce the estimation error from the original 15% down to

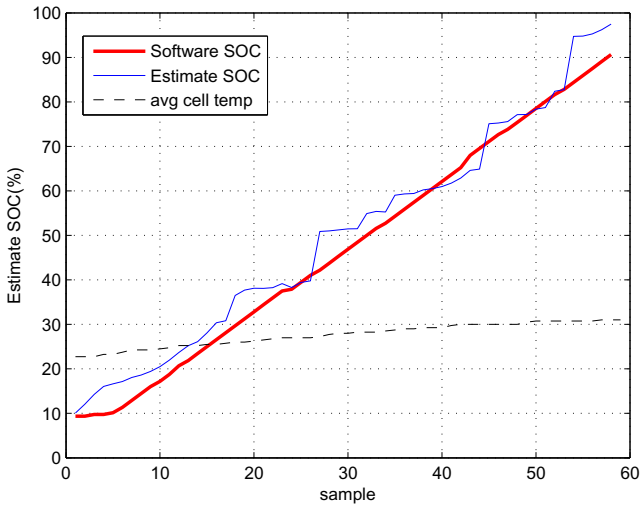

Figure 5.5: 30 Second Switch-off Time for SOC Estimation When Battery is Charging with Average Time Constant of 35 Second

Table 5.2: Battery Module SOC Estimation Result

Battery Module Test	Max Error (%)	Min Error (%)	Mean Error (%)	RMSD	Switch-off time (sec)
Charging (τ=44)	8.67	0.03	3.34	4.07	30
Discharging (τ=28)	9.88	0.08	3.22	3.86	30
Charging (τ=44)	8.66	0.07	3.26	3.87	60
Discharging (τ=28)	9.34	0.14	3.04	3.68	60

4% and it is apparent that a reasonable estimate of the SOC can be obtained with a 30 second switch-off time.

Improved SOC estimation for the single cell $LiFePO_4$ battery through the use of the time-constant is verified utilizing the same estimation procedure as the battery module. The time constant is chosen at the optimal point where RMSD is minimal. Fig.5.13 displays the resulting RMSD for the single cell battery. The optimal time constant for discharging is at 25 seconds while charging is 64 seconds. Fig. 5.14, Fig. 5.15 and Table 5.3 show the actual SOC and estimated SOC curve by using the chosen time constant.

The single cell battery also shows improvement in SOC estimation, especially in the charging test, compared to the original experiment. During the charging test, the SOC

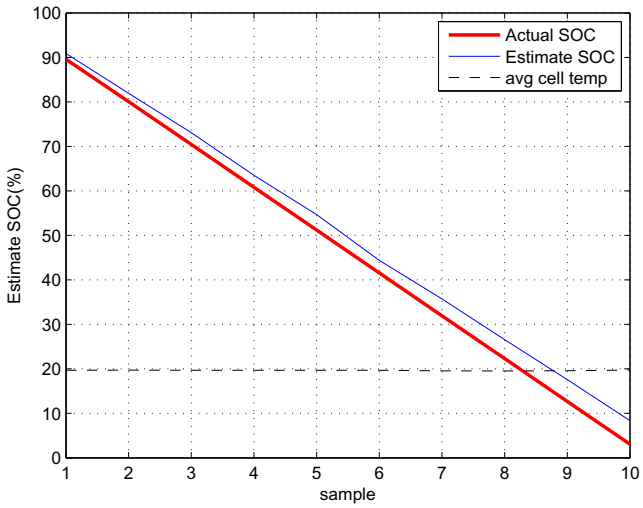

Figure 5.6: Single Cell Battery SOC Estimation: 30 Second Switch-off Time, Discharging Test with Average Time Constant of 33 Second

Table 5.3: Single Cell SOC Estimation Result

Single Cell Test	Max Error (%)	Min Error (%)	Mean Error (%)	RMSD	Switch-off time (sec)
Charging (τ=64)	2.56	0.37	1.37	1.40	30
Discharging (τ=25)	5.25	0.49	2.42	1.92	30
Charging (τ=64)	3.60	0.03	2.08	2.02	60
Discharging (τ=25)	5.27	0.16	2.13	2.96	60

estimation error is reduced from a maximum error of 10% down to 3%. Although the improvement is minimal for the discharging test, the estimation error is still under 5%. This demonstrates that the switch-off method for estimating SOC can be improved upon by augmenting a time-constant-based prediction of the OCV. This approach preserves the original goal of minimizing the need of complicated mathematical models of the lithium ion battery for SOC estimation.

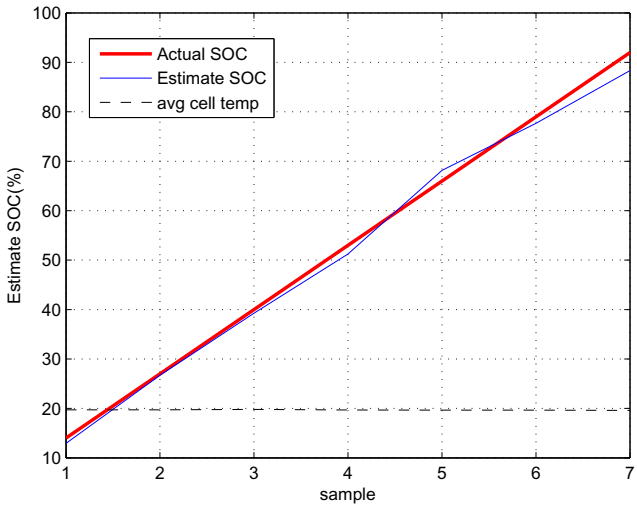

Figure 5.7: Single Cell Battery SOC Estimation: 30 Second Switch-off Time, Charging Test with Average Time Constant of 32 Second

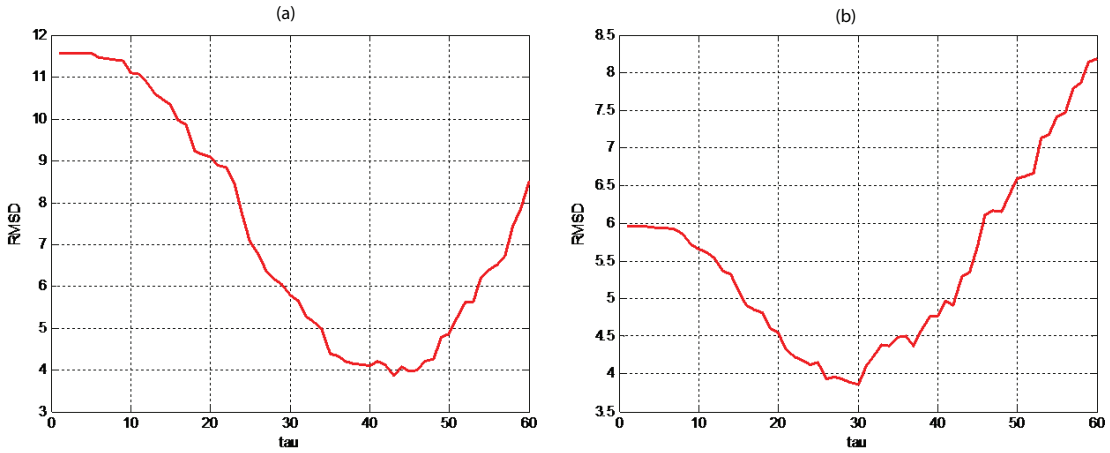

Figure 5.8: Battery Module RMSD Results (a) RMSD for Charging Time Constant, (b) RMSD Discharging Time Constant

5.3 Effect of Battery Aging on Time Constant

A drastic change in battery behavior such as its OCV recovery time may take place due to aging. To understand this phenomenon better, a battery-life testing is conducted the same way as in Section 5.1.2 for the single cell $LiFePO_4$ battery. The single cell battery is cycled over 500 times. The setup was used to monitor the variation in the time constant parameter

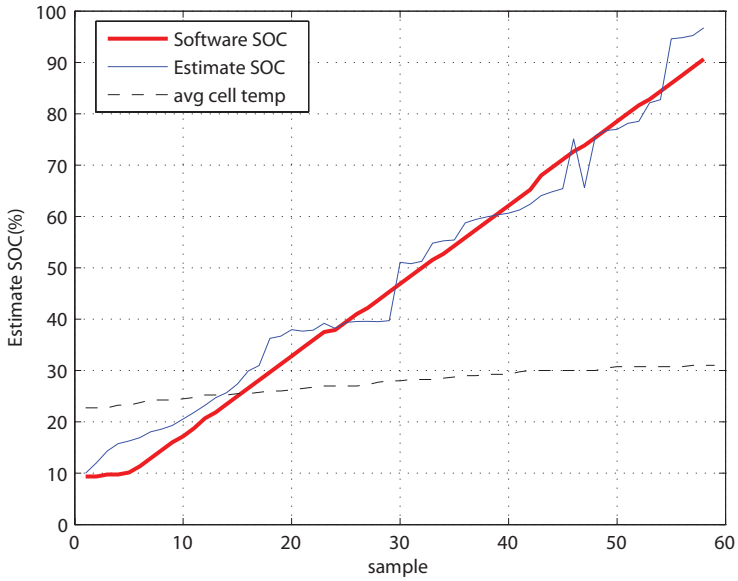

Figure 5.9: 60 Second Switch-off Time for SOC Estimation When Battery is Charging, with Ideal Time Constant

variation over cycles that emulate usage and aging. Earlier results showed that the battery's life cycle can have an effect on the time constant, based on the observation in Fig. 5.3. During the discharging test, at the lower SOC, the time constant varies up to 13 seconds as shown in Fig. 5.16. Between cycles in the 20s and the 200s, the time constant increases about 10 seconds at 7% SOC and an overall increase of 5% on average. During the charging test, Fig. 5.17 illustrates the cycles in the 20s and 200s. However, the variation does not have a clear trend compared to the discharging test.

From the data shown in Fig. 5.16, time constants at low SOC (20%), mid SOC (50%) and high SOC (90%) are isolated and their variation over cycles is plotted. Fig. 5.18 illustrates the time constant over different discharging cycles for 20, 50 and 90 % SOC. The data shows that at higher SOC, the time constant is consistent over 500 cycles. At lower SOC, the time constant actually decreases as the battery is cycled. Likewise, the comparison of charging tests over different cycles is presented in Fig. 5.19. Regardless of low, mid or high SOC, the overall time constant increases through the cycle life of the battery. The hysteresis effect is most likely a cause of the difference between charging and

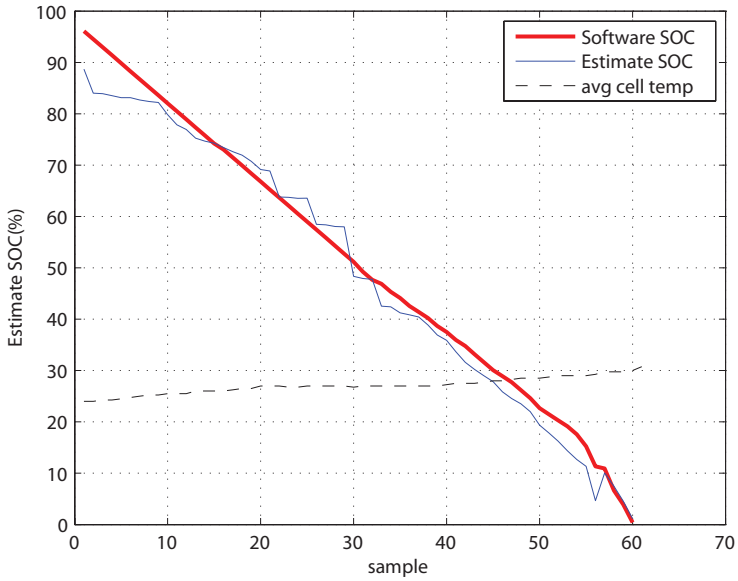

Figure 5.10: 60 Second Switch-off Time for SOC Estimation When Battery is Discharging, with Ideal Time Constant

discharging results.

Fig. 5.20 shows the comparison between cycle numbers 25 and 530 of the RMSD plot. The time constant with minimum RMSD is at about 28 for both cycles. This indicates that the chosen single time constant to estimate SOC may not change significantly over certain range of cycles. The SOC estimation of cycle 530 is shown in Fig. 5.21 and 5.22. The plots are generated by using the ideal time constant. The result is still accurate even with an aged battery after 500 cycles. The calculated time constant may indicate the age of the battery. However, further investigation is needed for a complete understanding of the relationship between the battery's age and the corresponding time constant of the slow transient of the terminal voltage.

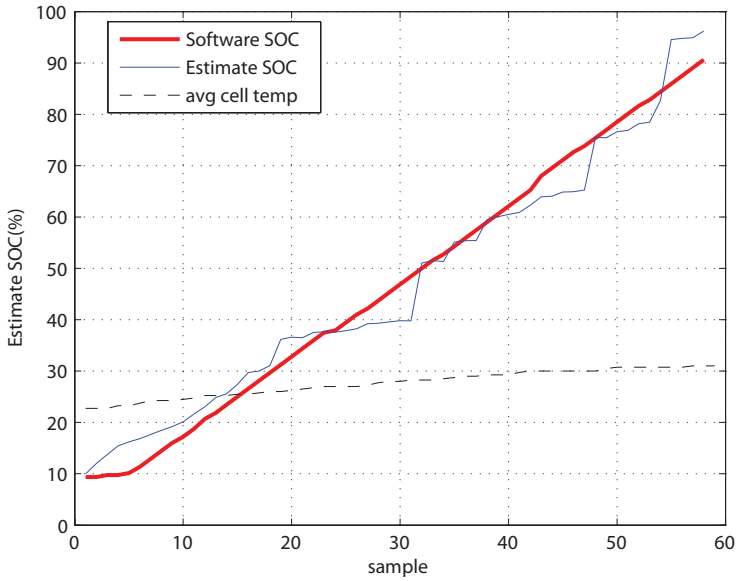

Figure 5.11: 30 Second Switch-off Time for SOC Estimation When Battery is Charging, with Ideal Time Constant

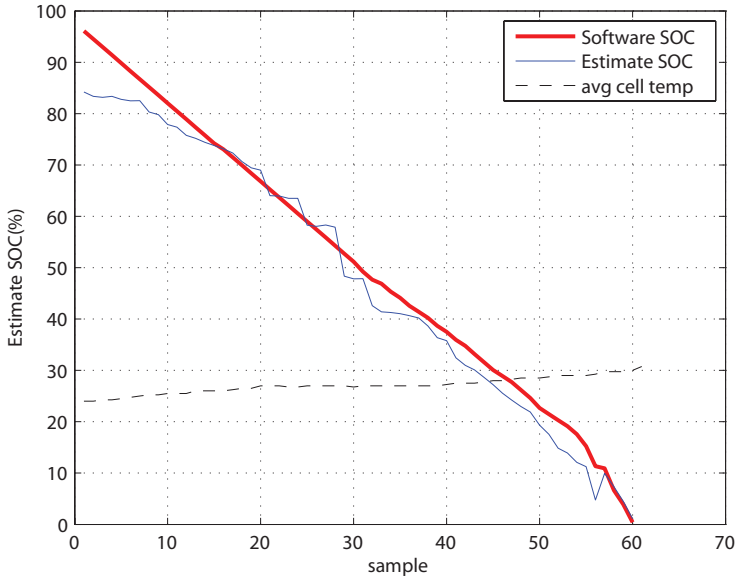

Figure 5.12: 30 Second Switch-off Time for SOC Estimation When Battery is Discharging, with Ideal Time Constant

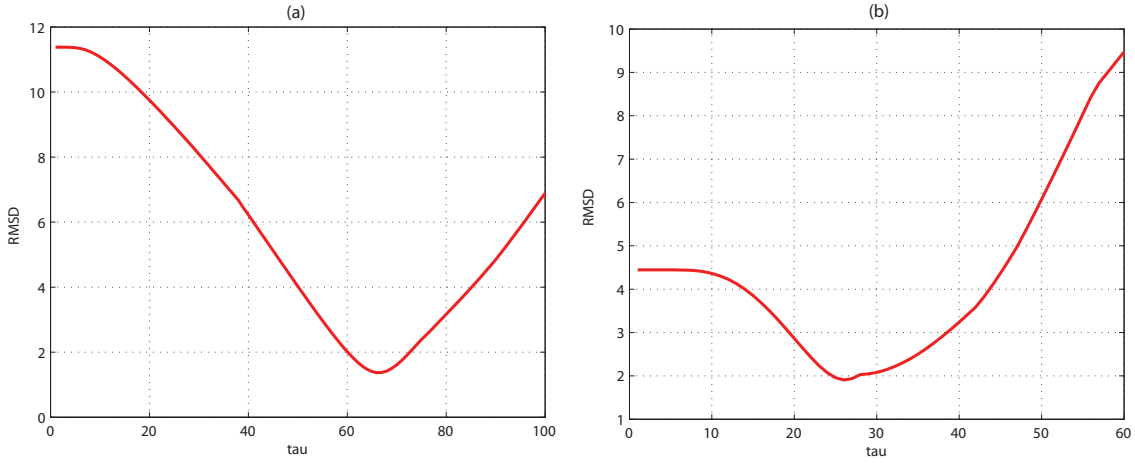

Figure 5.13: Single Cell Battery RMSD Results (a) RMSD for Charging Time Constant, (b) RMSD Discharging Time Constant

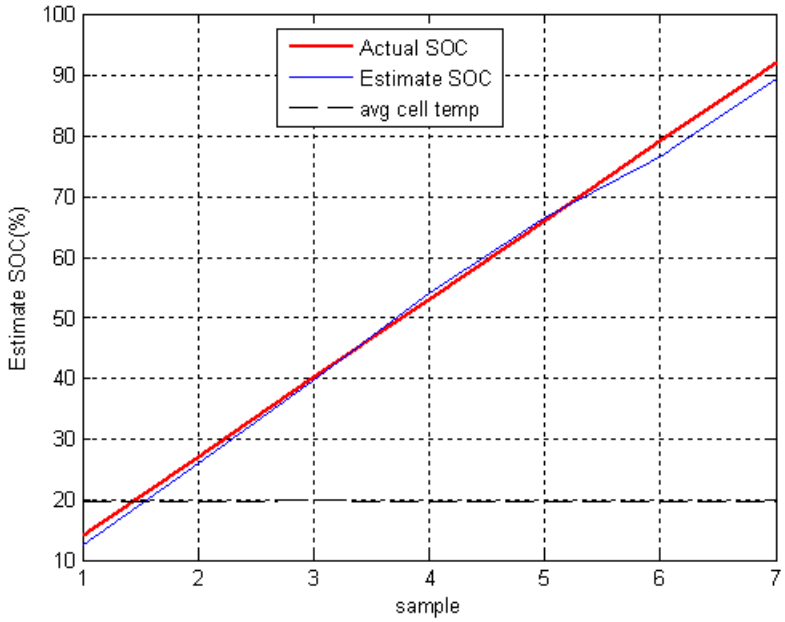

Figure 5.14: 30 Second Switch-off Time for SOC Estimation When Battery is Charging, with Ideal Time Constant

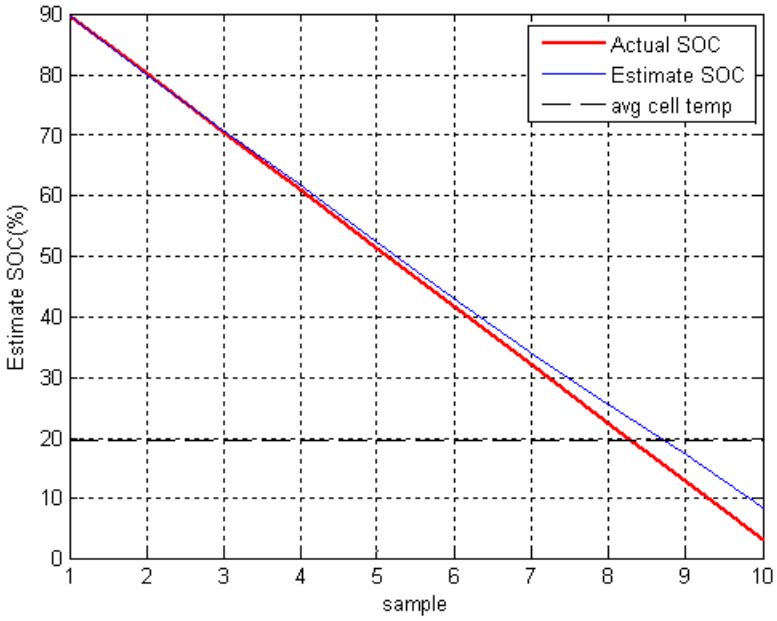

Figure 5.15: 30 Second Switch-off Time for SOC Estimation When Battery is Discharging, with Ideal Time Constant

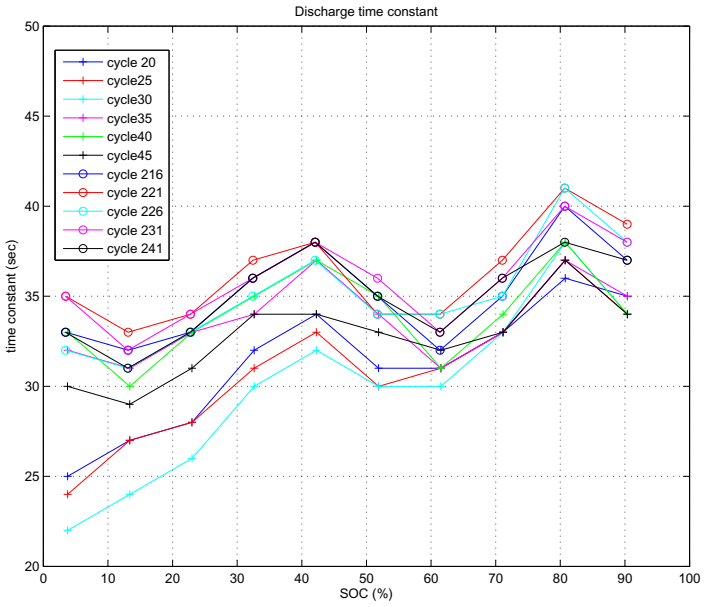

Figure 5.16: Discharge Time Constant Comparison Between Cycles

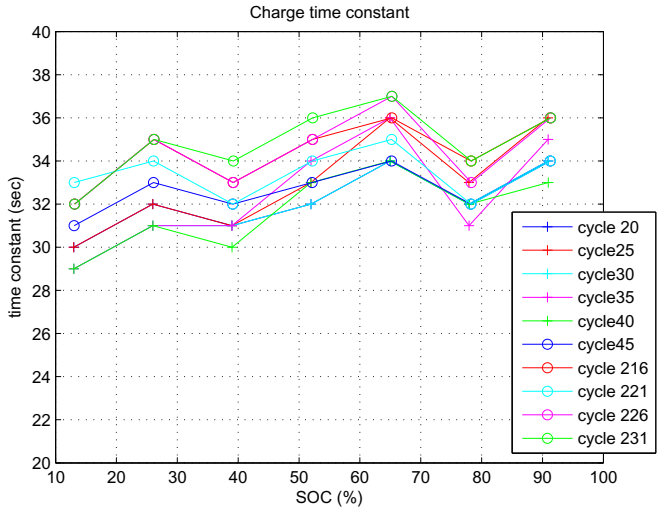

Figure 5.17: Charge Time Constant Comparison Between Cycles

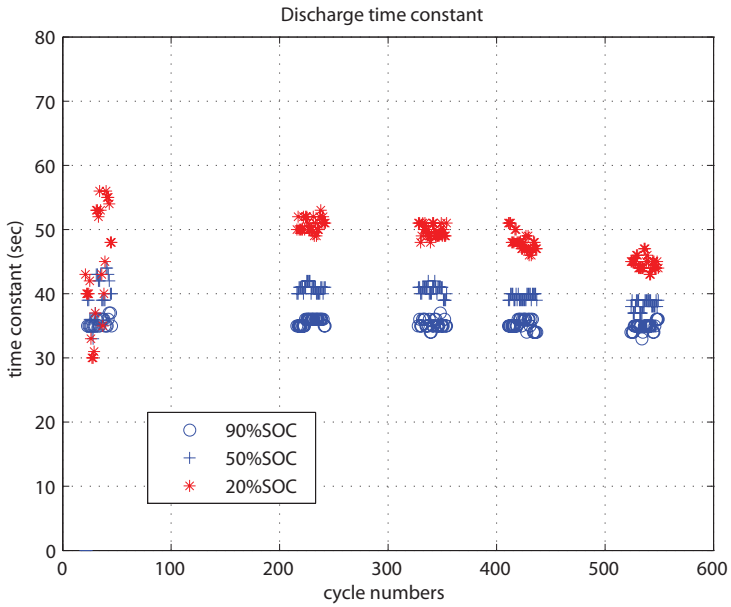

Figure 5.18: Discharge Time Constant Over Cycles

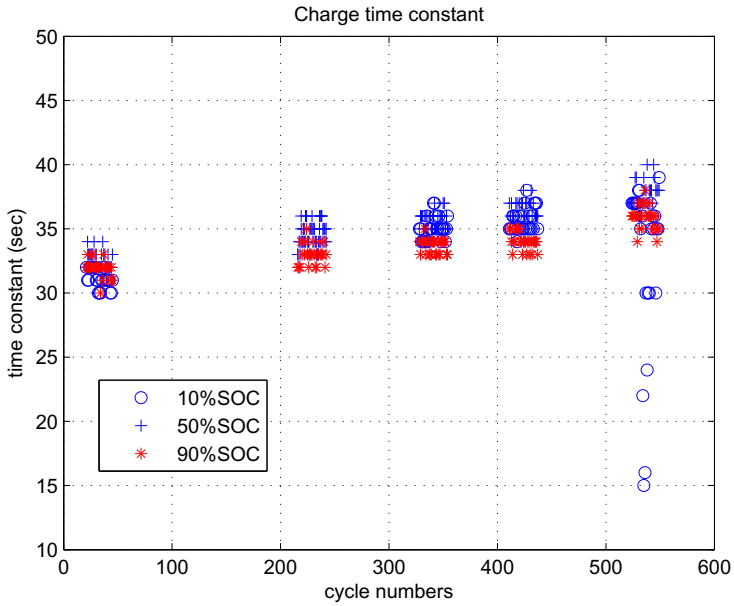

Figure 5.19: Charge Time Constant Over Cycles

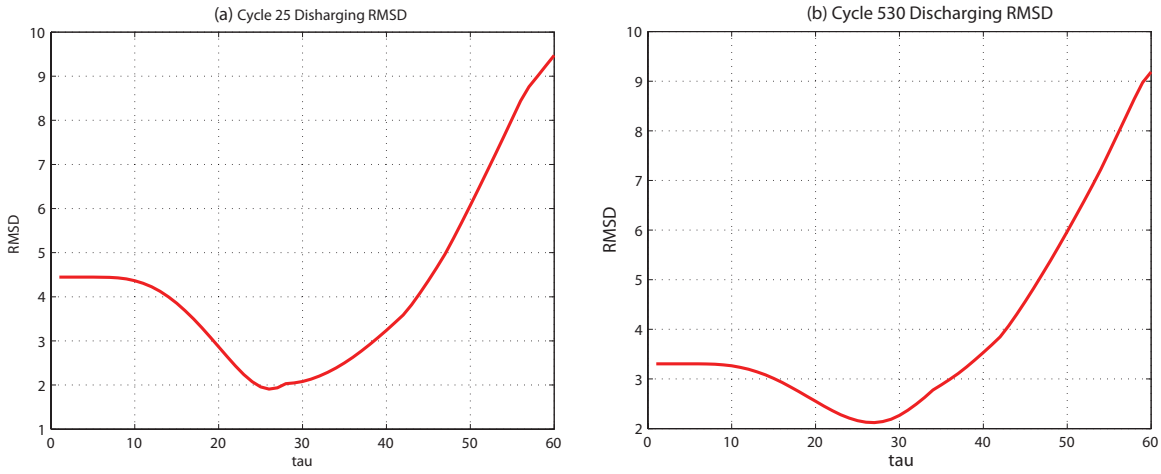

Figure 5.20: A123 LiFePO4 Battery Cycle Number RMSD Comparison

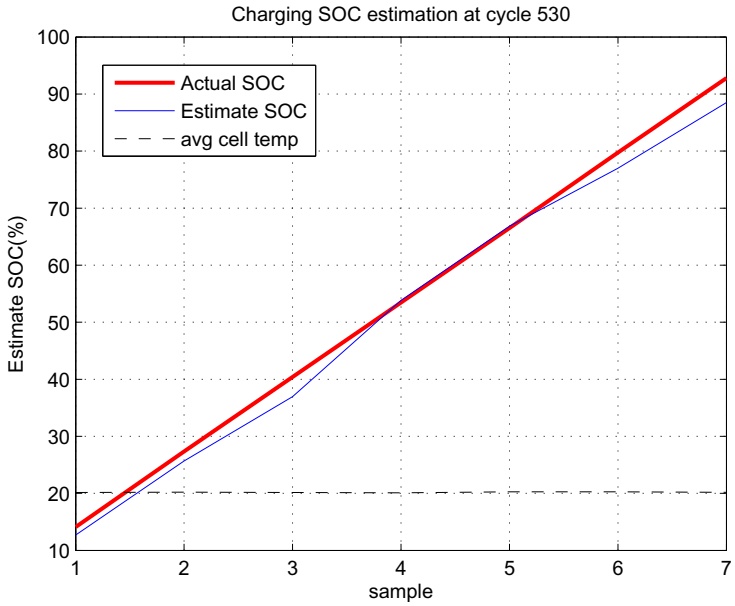

Figure 5.21: SOC Estimation When Battery is Charging at Cycle 530

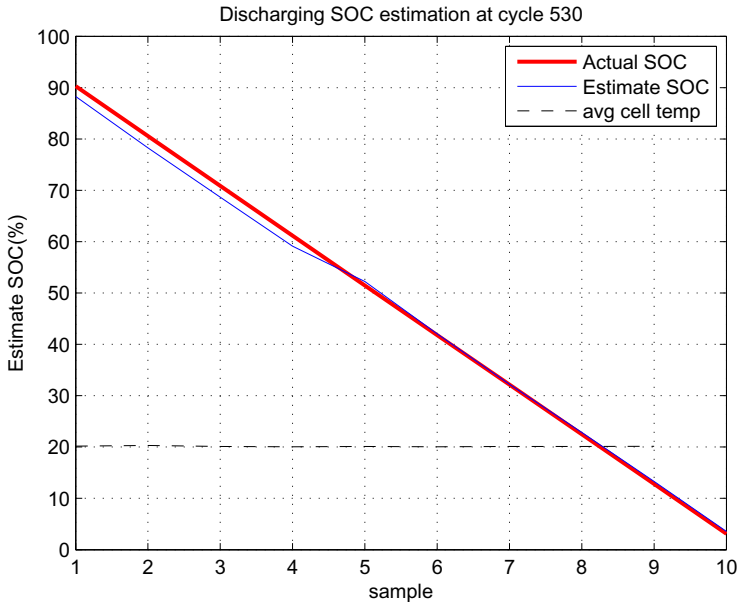

Figure 5.22: SOC Estimation When Battery is Discharging at Cycle 530

Chapter 6

Conclusion

This thesis investigates a switching-based approach for SOC estimation for Li-ion batteries. The concept behind the proposed estimation approach is to switch off the battery intermittently and measure the terminal voltage during the switch-off durations. Such intermittent switch-off intervals could be feasible in hybrid energy scenarios where multiple storage elements are connected. Once switched off, the terminal voltage approaches the OCV. In Li-ion batteries, this transient was found to be faster compared to conventional lead-acid batteries. The fast transient is advantageous as it implies that a small switch-off duration could provide a reasonably accurate measure of the OCV. This estimated OCV can then be used to estimate the SOC with the help of an OCV vs. SOC mapping, which is a characteristic property of a battery. The proposed OCV measurement approach can generate a large error if the switch-off time is too short. Hence, the thesis experimentally probes the trade-off between switch-off times and OCV measurement error. Whether the battery was charging or discharging, application of the correct OCV vs. SOC curve can minimize the SOC estimation error. The OCV vs. SOC curves were found to be slightly different during charging and discharging cycles. The disparity is possibly due to the hysteresis effect of the battery.

Even when applying the appropriate OCV vs. SOC curve, the error can be as large as 15% for a 30 second waiting time - increasing beyond 15% as the switch-off time decreases. Next, it is observed that the transient response of the battery terminal voltage during switch-off is composed of two transient effects. Initially, there is a sharp (almost

instantaneous) recovery of the terminal voltage, of a high magnitude. This is followed by a slower transient of lower magnitude. With this observation, we propose to approximate the slower transient using a first-order behavior and estimate its time constant during the switch-off interval. Utilizing a single time constant for charging and one for discharge, obtained from experiments, the SOC estimation error is reduced to 5% over the entire range of SOC, for a 30 second wait time. The single time constant methodology demonstrates a more accurate SOC estimation without the need of precise laboratory equipment or an extended switch-off time or a complicated and precise model of the battery. It was also apparent that the age of the battery has minimal impact on the time constant used for SOC estimation.

This thesis, however, discovered that the time constant changes over usage. Over 500 cycles, there is an approximately five second of time constant increase during charging and five second decrease during discharging. As the battery is cycled, it is noted that the time constant increases as the battery ages during charging tests. During discharge tests, a clear trend of variation of the time constant was not observed. Further investigation is required to determine the relationship between the battery's age and the time constant for the aforementioned slow transient of the terminal voltage of Li-ion batteries during switch-off.

For both the single cell battery and the 12V battery module, the SOC estimation method using a time constant shows promise of being applicable in control applications. As long as the system allows the battery to switch off from the circuit for a short period of time, or is in a parallel configuration, the switching-based SOC sensing technique could serve as a simple sensing/estimation approach, obviating the need for complicated model development. The most immediate opportunity for future work is to utilize the SOC estimation method in control applications; for example, in hybrid energy systems. The switching-based sensing investigated in this thesis can be applied in fuel cell/battery hybrid energy systems. Hybridizing the power source and battery together can optimize energy usage within the system [54][58].

References

[1] J. M. Tarascon and M. Armand. Issues and challenges facing rechargeable lithium batteries. *Nature International Weekly Journal of Science*, 414:359–367, November 2001.

[2] A. Yamada, S. C. Chung, and K. Hinokuma. Optimized $LiFePO_4$ for lithium battery cathodes. *Journal of The Electrochemical Society*, 148(3):A224–A229, 2001.

[3] O. Toprakci, H. A. K. Toprakci, L. Ji, and X. Zhang. Fabrication and electrochemical characteristics of $LiFePO_4$ powders for lithium-ion batteries. *KONA Powder and Particle Journal*, (28):50–73, 2010.

[4] D. Di Domenico, G. Fiengo, and A. G. Stefanopoulou. Lithium-ion battery state of charge estimation with a kalman filter based on a electrochemical model. In *Proc. IEEE International Conference on Control Applications CCA*, pages 702–707, September 2008.

[5] Y. He, W. Liu, and B.J. Koch. Battery algorithm verification and development using hardware-in-the-loop testing. *Journal of Power Sources*, 195:2969–2974, 2010.

[6] http://www.a123systems.com/.

[7] T. Allag. Robust control strategies for hybrid solid oxide fuel cell systems. Master's thesis, Rochester Institute of Technology, 2010.

[8] http://www.grainger.com/.

[9] W. Dreyer, J. Jaminik, C. Guhlke, R. Huth, J. Moskon, and M. Gaberscek. The thermodynamic origin of hysteresis in insertion batteries. *Nature Materials*, 9:448–453, April 2010.

[10] S. Piller, M. Perrin, and A. Jossen. Methods for state-of-charge determination and their applications. *Journal of Power Sources*, 96(1):113–120, january 2001.

[11] V. Pop, H. J. Bergveld, P. H. L. Notten, and P. P. L. Regtien. State-of-the-art of battery state-of-charge determination. *Measurement Science and Technology*, 16:93–110, December 2005.

[12] R. Brood. *Lithium Mobile Power, Advances in Lithium Battery technologies for Mobile applications*. Knowledge Press, Inc., 18 Webster St, Brookline, MA02446, 3 edition, 2009.

[13] P. G. Balakrishnan, R. Ramesh, and T. Prem Kumar. Safety mechanisms in lithium-ion batteries. *Journal of Power Sources*, 155:401414, February 2006.

[14] M. Winter and R. J. Brodd. What are batteries, fuel cells, and supercapacitors? *Chemical review, American Chemical Society*, 104(10):4245–4269, September 2004.

[15] M. Coleman, W. G. Hurley, and C. K. Lee. An improved battery characterization method using a two-pulse load test. *Energy Conversion, IEEE Transactions on*, 23(2):708 –713, 2008.

[16] K. S. Ng, C. S. Moo, Y. P. Chen, and Y. C. Hsieh. Enhanced coulomb counting method for estimating state-of-charge and state-of-health of lithium-ion batteries. *Journal of Applied Energy*, 86:1506–1511, November 2009.

[17] T. Hansen and C.J. Wang. Support vector based battery state of charge estimator. *Journal of Power Sources*, 141(2):351 – 358, 2005.

[18] V. Pop, H. J. Bergveld, J. H. G. Veld op het, P. P. L. Regtien, D. Danilov, and P. H. L. Notten. Modeling battery behavior for accurate state-of-charge indication. *Journal of the Electrochemical Society*, 153(11):A2013–A2022, 2006.

[19] T. Hirai, A. Ohnishi, N. Nagaoka, N. Mori, A. Ametani, and S. Umeda. Automatic equivalent-circuit estimation system for lithium-ion battery. In *Universities Power Engineering Conference, 2008. UPEC 2008. 43rd International*, pages 1 –5, 2008.

[20] M. Chen and G. A. Rincon-Mora. Accurate electrical battery model capable of predicting runtime and i-v performance. *Energy Conversion, IEEE Transactions on*, 21(2):504 – 511, 2006.

[21] A. Banaei, A. Khoobroo, and B. Fahimi. Online detection of terminal voltage in li-ion batteries via battery impulse response. In *Vehicle Power and Propulsion Conference, 2009. VPPC '09. IEEE*, pages 194 –198, 2009.

[22] M. Coleman, C. K. Lee, and W. G. Hurley. State-of-charge determination from EMF voltage estimation: Using impedance,terminal voltage, and current for lead-acid and lithium-ion batteries. *IEEE Transactions On Industrial Electronics*, 54(5):2550–2556, October 2007.

[23] J. Kim, S. Lee, and B. Cho. Discrimination of battery characteristics using discharging/charging voltage pattern recognition. In *2009 Energy Conversion Congress and Exposition*, pages 1799 – 1805. Institute of Electrical and Electronics Engineers Inc., September 2009.

[24] P. Rong and M. Pedram. An analytical model for predicting the remaining battery capacity of lithium-ion batteries. *IEEE Transactions on Very Large Scale Integration (VLSI) systems*, 14(5):441–451, May 2006.

[25] A. Szumanowski and Y. Chang. Battery management system based on battery nonlinear dynamics modeling. *Vehicular Technology, IEEE Transactions on*, 57(3):1425 –1432, May 2008.

[26] S. Rodrigues, N. Munichandraiah, and A. K. Shukla. A review of state-of-charge indication of batteries by means of a.c. impedance measurements. *Journal of Power Sources*, 87(1-2):12 – 20, 2000.

[27] A. Jossen. Fundamentals of battery dynamics. *Journal of Power Sources*, 154(2):530 – 538, 2006. Selected papers from the Ninth Ulm Electrochemical Days.

[28] K. Smith and C. Y. Wang. Power and thermal characterization of a lithium-ion battery pack for hybrid-electric vehicles. *Journal of Power Sources*, 160:662–673, February 2006.

[29] K. Smith and C. Y. Wang. Solid-state diffusion limitations on pulse operation of a lithium ion cell for hybrid electric vehicles. *Journal of Power Sources*, 161:628–639, March 2006.

[30] C. Speltino, D. Di Domenico, G. Fiengo, and A. G. Stefanopoulou. On the experimental identification of an electrochemical model of a lithium-ion battery: Part ii. In *The European Control Conference*, 2009.

[31] M. A. Roscher, J. Vetter, and D. U. Sauer. Characterization of charge and discharge behaviour of lithium ion batteries with olivine based cathode active material. *Journal of Power Sources*, 191:582–590, February 2009.

[32] S. Santhanagopalan and R.E. White. Online estimation of the state of charge of a lithium ion cell. *Journal of Power Sources*, 161(2):1346 – 1355, 2006.

[33] C. Speltino, D. Di Domenico, G. Fiengo, and A. G. Stefanopoulou. Comparison of reduced order lithium-ion battery models for automotive applications. In *Joint 48th IEEE Conference on Decision and Control and 28th Chinese Control Conference*, October 2009.

[34] K. Ozawa. *Lithium Ion Rechargeable batteries*. Wiley-VCH, 1 edition, 2009.

[35] Y. P. Chen K. S. Ng, C. S. Moo and Y. C. Hsieh. State-of-charge estimation for lead-acid batteries based on dynamic open-circuit voltage. In *IEEE Conference on Power and Energy*, December 2008.

[36] S. Lee, J. Kim, J. Lee, and B. H.Cho. State-of-charge and capacity estimation of lithium-ion battery using a new open-circuit voltage versus state-of-charge. *Journal of Power Sources*, 185:1367–1373, September 2008.

[37] Y Tanjo, T Nakagawa, H Horie, T Abe, K Iwai, and M Kawai. State of charge indicator US patent 6127806, 14 May 1999.

[38] Z. Jiang and R. A.Dougal. Real-time strategy for active power sharing in a fuel cell powered battery charger. *Journal of Power Sources*, 142:253–263, December 2004.

[39] J. Xu, M. Gao, Z. He, J. Yao, and H. Xu. Design and study on the state of charge estimation for lithium-ion battery pack in electric vehicle. In *Artificial Intelligence and Computational Intelligence, 2009. AICI '09. International Conference on*, volume 3, pages 316 –320, 2009.

[40] B. T. Kuhn, G. E. Pitel, and P. T. Krein. Electrical properties and equalization of lithium-ion cells in automotive applications. In *Vehicle Power and Propulsion, 2005 IEEE Conference*, page 5 pp., 2005.

[41] I.S. Kim. Nonlinear state of charge estimator for hybrid electric vehicle battery. *Power Electronics, IEEE Transactions on*, 23(4):2027 –2034, 2008.

[42] I. S. Kim. The novel state of charge estimation method for lithium battery using sliding mode observer. *Journal of Power Sources*, 163(1):584 – 590, 2006. Special issue including selected papers presented at the Second International Conference on Polymer Batteries and Fuel Cells together with regular papers.

[43] J. Kim, S. Lee, and B. Cho. The determination of state of charge based on extended kalman filter using per-unit system and time constant principle. In *Telecommunications Energy Conference, 2009. INTELEC 2009. 31st International*, pages 1 –5, 2009.

[44] L. Gao, S. Liu, and R. A. Dougal. Dynamic lithium-ion battery model for system simulation. *Components and Packaging Technologies, IEEE Transactions on*, 25(3):495 – 505, September 2002.

[45] R. C. Kroeze and P. T. Krein. Electrical battery model for use in dynamic electric vehicle simulations. In *Power Electronics Specialists Conference, 2008. PESC 2008. IEEE*, pages 1336 –1342, 2008.

[46] J. Kim, S. Lee, and B. Cho. The state of charge estimation employing empirical parameters measurements for various temperatures. In *Power Electronics and Motion Control Conference, 2009. IPEMC '09. IEEE 6th International*, pages 939 –944, May 2009.

[47] S. Abu-Sharkh and D. Doerffel. Rapid test and non-linear model characterisation of solid-state lithium-ion batteries. *Journal of Power Sources*, 130:266–274, December 2004.

[48] S. J. Lee, J. H. Kim, J. M. Lee, and B. H. Cho. The state and parameter estimation of an li-ion battery using a new ocv-soc concept. In *Power Electronics Specialists Conference, 2007. PESC 2007. IEEE*, pages 2799 –2803, 2007.

[49] M. H. Nehrir and C. Wang. *Modeling and Control of Fuel Cells - Distributed Generation Applications*. John Wiley and Sons, Inc., 2009.

[50] Maxim application note 121. Inaccuracies of estimating remaining cell capacity with voltage measurements alone, May 2002.

[51] M. S. Whittingham. Lithium batteries and cathode materials. *Chemical Reviews*, 104(10):4271–4302, 2004.

[52] J. Chen and M. Stanley Whittingham. Hydrothermal synthesis of lithium iron phosphate. *Electrochemistry Communications*, 8(5):855 – 858, 2006.

[53] C. S. Moo, K. S. Ng, Y. P. Chen, and Y. C. Hsieh. State-of-charge estimation with open-circuit-voltage for lead-acid batteries. In *Power Conversion Conference - Nagoya, 2007. PCC '07*, pages 758 –762, april 2007.

[54] O. Sundstrom and A. Stefanopoulou. Optimal power split in fuel cell hybrid electric vehicle with different battery sizes, drive cycles, and objectives. In *Proc. IEEE Computer Aided Control System Design IEEE International Conference on Control Applications IEEE International Symposium on Intelligent Control*, pages 1681–1688, 4–6 Oct. 2006.

[55] U-charger rt battery module user's guide. pages 1–24, 2008.

[56] C. Speltino, D. Di Domenico, G. Fiengo, and A. G. Stefanopoulou. Cell equalization in battery stacks through state of charge estimation polling. In *American Control Conference*, 2010.

[57] M. A. Roscher and D. U. Sauer. Dynamic electric behavior and open-circuit-voltage modeling of lifepo4-based lithium ion secondary batteries. *Journal of Power Sources*, 196(1):331 – 336, 2011.

[58] M. J. Kim and H. Peng. Power management and design optimization of fuel cell/battery hybrid vehicles. *Journal of Power Sources*, 165(2):819 – 832, 2007.

Appendix A

Simulink and Control-Desk interfacing

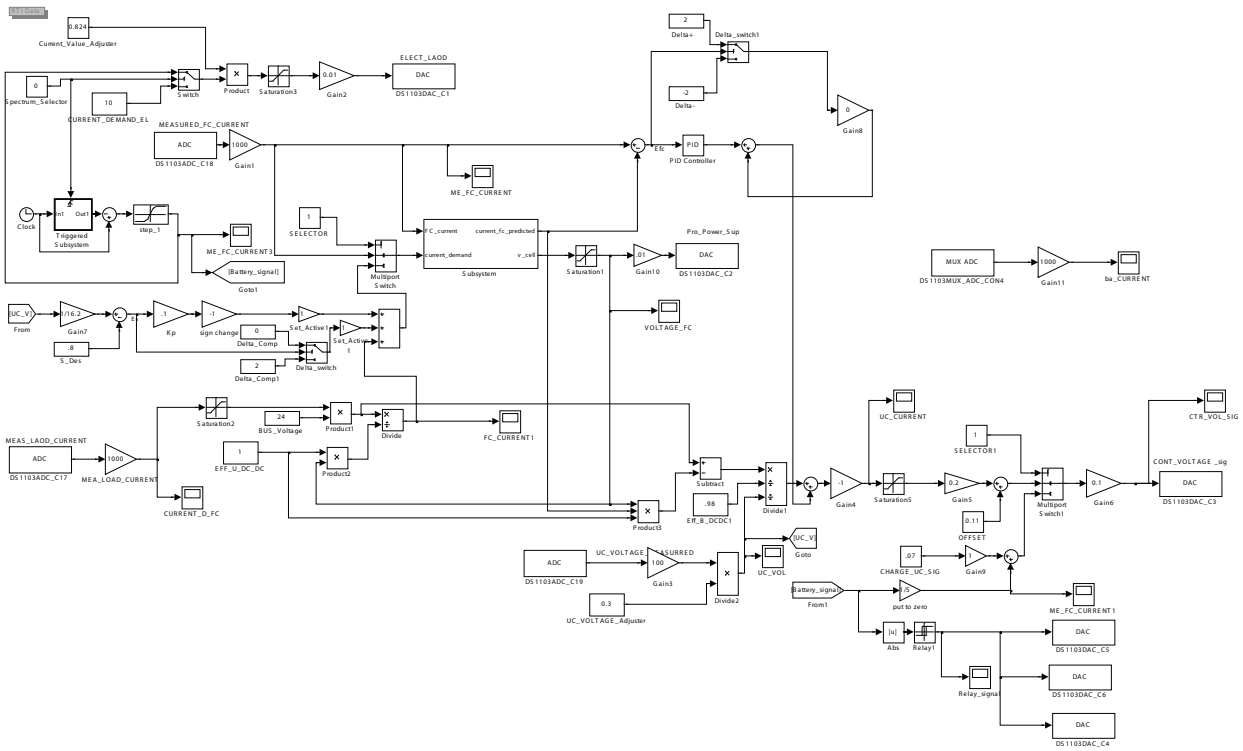

Figure A.1: The Overall Simulink Model of the Battery testing experiment

The Simulink setup for the battery testing is presented in Fig.A.1 is shown in A.1. This setup is a modified version of the pre-existing simulink model provided by [7]. As mentioned in Section 3.1, dSPACE is used for monitoring the hardware data. All the sensor

inputs and control outputs shown in Fig.A.1 are interfaced through dSPACE. The dSPACE monitoring GUI is shown in Fig.A.2

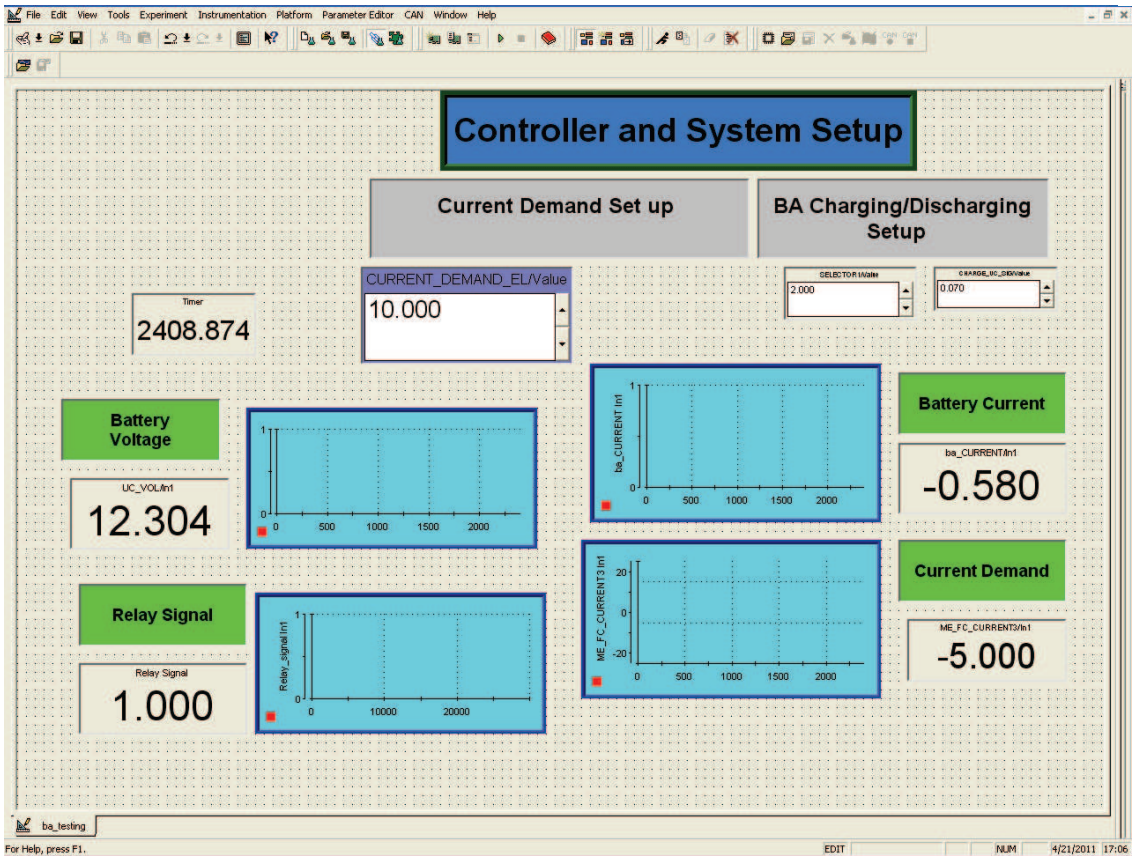

Figure A.2: Battery testing Setup Using Control-Desk Interface Software

Appendix B

Matlab Code for Battery Testing

The following MATLAB code is used to set up the testing timing for the charging and discharging experiment of the battery module. The MATLAB code is loading into DSPACE for real time hardware testing.

$VocTime = 300; \quad chargingTime = 120; \quad dischargingTime = 120; \quad Acharge = 20; \quad Adischarge = 20; \quad s = 1; \quad N = VocTime;$

$for \quad k = 0 : 1 : 30$

$for \quad i = s : 1 : N$

$TimeSOC(i) = i - m; StepSOC(i) = 0;$

end

$for \quad i = N + 1 : 1 : (N + dischargingTime) + 1$

$TimeSOC(i) = i - m - 1; \quad StepSOC(i) = Adischarge;$

end

$for \quad i = (N+dischargingTime)+2 : 1 : (VocTime+dischargingTime+N)+2$

$TimeSOC(i) = i - 2 - m; \quad StepSOC(i) = 0;$

end

$for \quad i = (VocTime+dischargingTime+N)+3 : 1 : (VocTime+dischargingTime+N + chargingTime) + 3$

$TimeSOC(i) = i - 3 - m;$

$StepSOC(i) = Acharge;$

end

$s = (k+1) * (2 * VocTime + dischargingTime + chargingTime + 3) + k + 1;$

$N = s + (k+1) * VocTime - k * VocTime;$

$m = 3 * (k+1) + (k+1);$

end